Imaging Neuroscience
an open access journal

Research Article

Multimodal neuroimaging of fatigability development

Patrick Bedard[a], Kristine M. Knutson[b], Patrick M. McGurrin[a], Felipe Vial[c], Traian Popa[a], Silvina G. Horovitz[a], Mark Hallett[a], Avindra Nath[a], Brian Walitt[a]

[a]Human Motor Control Section, National Institute of Neurological Disorders and Stroke, National Institutes of Health, Bethesda, MD, United States
[b]Behavioral Neurology Unit, National Institute of Neurological Disorders and Stroke, National Institutes of Health, Bethesda, MD, United States
[c]Clínica Alemana Universidad del Desarrollo, Santiago, Chile

Corresponding Author: Patrick Bedard (patrick.bedard@nih.gov)

ABSTRACT

Fatigability refers to the inability of the neuromuscular system to generate enough force to produce movements to meet task challenges. Fatigability has a central and a peripheral component linked via the neuromuscular system, but how these two components interact as fatigue develops lacks a complete understanding. The effects of fatigability are experienced in healthy humans but also accompany various disorders, often exacerbating their symptoms. We studied how fatigability develops in the neuromuscular system using multimodal neuroimaging. We recruited healthy participants to perform a fatiguing grip force task, while recording force, electromyography of forearm muscles (EMG), electroencephalography (EEG), and functional magnetic resonance imaging (fMRI) in 30-second blocks of grip task alternating with 30 seconds of rest. The task entailed maintaining 50% of the maximum force. We combined EMG and EEG to compute corticomuscular coherence and combined EEG and fMRI to compute EEG-informed fMRI. We selected eight task blocks specific to each participant to represent how the neuromuscular system adapted from pre-fatigability to actual fatigability. Those included five blocks for pre-fatigability in which participants could generate enough force to match the required 50% of maximum force and three blocks when the force fell below that limit. Across blocks of the grip force task, we observed changes in the neuromuscular system that preceded grip force changes. We found that electromyography of arm muscles shifted from high to low frequency, EEG in the channel covering the contralateral sensorimotor area increased steadily up to the fifth block and then plateaued, and fMRI signal also increased in the cerebellum. Corticomuscular coherence increased within each of the 30-second blocks of the grip task. EEG-informed fMRI revealed areas of the brain that the traditional regression did not, including the bilateral sensorimotor cortex, temporal-parietal junction, and supplementary motor area. Thus, as fatigability developed, the neuromuscular system experienced changes earlier than the actual behavior. While we found evidence for fatigability of central and peripheral origins, peripheral fatigue seems to occur first.

Keywords: fatigability, fMRI, EEG, EMG, corticomuscular coherence

1. INTRODUCTION

Fatigability is a reduction of the output of the neuromuscular system that fails to generate enough force to elicit movement despite willed effort (Enoka & Duchateau, 2016). The feeling or perception of fatigability is referred to as fatigue (Kluger et al., 2013) and can be independent from fatigability. Fatigability can have both a central or peripheral origin within the neuromuscular system (Gandevia, 2001). Fatigue is a major complaint in many disorders, such as multiple sclerosis, movement disorders, cancer, and Myalgic-Encephalomyelitis/Chronic Fatigue Syndrome (ME/CFS) and can be quite debilitating

Received: 13 February 2025 Revision: 6 August 2025 Accepted: 9 August 2025 Available Online: 12 August 2025

(Kluger et al., 2013; Millet et al., 2023). The relation between fatigue and fatigability is still not well understood.

Prior work on fatigability of the neuromuscular system has mostly used a unimodal design. These studies have observed that fatigability is generally accompanied by a shift in the electromyography (EMG) power spectrum from high to low frequencies, resulting in a higher low/high frequency ratio. This has been well captured by a novel fatigability metric, the Dimitrov Index (DI; Dimitrov et al., 2006; Dimitrova et al., 2005; Zhao et al., 2022). Using a variety of study paradigms, studies with electroencephalography (EEG) have demonstrated increases in power in multiple frequency bands, including mu, beta, and gamma, across the sensorimotor, parietal, and prefrontal areas (Berchicci et al., 2013; Enders et al., 2016; Guo et al., 2014; Johnston et al., 2001; Schillings et al., 2006; Suviseshamuthu et al., 2022; Wang et al., 2017). Functional magnetic resonance imaging (fMRI) studies have reported an increase in the blood oxygen level dependent (BOLD) signal in brain areas, including the sensorimotor cortex, cerebellum, and cingulate gyrus, during fatigability development (Benwell et al., 2007; Jiang et al., 2016; Liu et al., 2003; Post et al., 2009; van Duinen et al., 2007).

However, a broader understanding of fatigability should be possible by combining neurophysiologic and neuroimaging techniques. To date, multimodal neuroimaging with EMG, EEG, and fMRI to study fatigability has received little attention. Combining EEG with EMG allows for corticomuscular coherence (CMC) to be studied (Liu et al., 2019; Mima & Hallett, 1999). Combining EEG with fMRI allows for EEG-informed fMRI measurements (Abreu et al., 2018).

CMC reflects the synchronous and rhythmic electrical activity in both the primary motor cortex and the contralateral muscle fibers during movement. This activity occurs mostly in the ~13–30 Hz range (beta band) but also in the ~30–50 Hz range (gamma band) (Baker et al., 1997; Conway et al., 1995); reviews in Liu et al. (2019); and Mima and Hallett (1999). Also, CMC has a directionality component with an efferent (brain to muscles) and an afferent (muscles to brain) component (Witham et al., 2011). Each frequency band and directionality component likely subserve different aspects of motor control. The beta band appears to be involved in maintaining steady-state motor output, such as seen during an isometric contraction, while the gamma band appears to be involved in dynamic force generation, such as seen during an isotonic contraction (Gwin & Ferris, 2012; Mehrkanoon et al., 2014; Omlor et al., 2011; Ushiyama et al., 2017). Further, the gamma band appears to be more involved with the afferent component of CMC, as evidenced by a deafferented patient showing no gamma band CMC (Patino et al., 2008). Fatigability can affect CMC in the beta and gamma bands (Hsu et al., 2023; Liang et al., 2021; Siemionow et al., 2010; Tecchio et al., 2006; Tuncel et al., 2010; Ushiyama et al., 2011; Yang et al., 2009). However, results regarding CMC have been inconsistent, due to various factors including experimental design, task selection, force intensity, and data preprocessing. A major issue in many of these studies is that fatigability is not measured as it is occurring. In general, measures are collected before and after a fatiguing task, rather than during the development of fatigability. One study that did measure fatigability in real time noted a significant reduction in CMC (Siemionow et al., 2010). Finally, one study using the before and after design did assess the directionality of CMC information flow with fatigability, reporting that beta efferent was less strong after the fatiguing task while beta afferent was stronger (Liang et al., 2021). Multimodal approaches have the potential to broaden CMC understanding as it relates to fatigability.

EEG-informed fMRI measurements have not yet been applied to the study of fatigability (reviews in Abreu et al., 2018; Warbrick, 2022). In a typical block design fMRI experiment, the hemodynamic response function (HRF) that is used to estimate the task regressor of the BOLD signal is held constant across trial blocks and individuals. In EEG-informed fMRI, the EEG features are used to modulate the height of the HRF (Ataei et al., 2024; Horovitz et al., 2004; Scheeringa et al., 2016). EEG-informed fMRI allows for both positive and negative associations between the EEG and fMRI, depending on the frequency bands and brain areas (Goldman et al., 2002; Kilner et al., 2005; Laufs et al., 2003; Scheeringa et al., 2016). The richer and more complex models of EEG-informed fMRI can lead to better understanding of cognitive processes.

Here, we aim to study the development of fatigability and how it is represented in the neuromuscular system. We were especially interested to study how corticomuscular coherence and its directionality and EEG-informed fMRI change during the development of fatigability. While prior work did assess fatigability with various metrics including EMG, EEG, and fMRI, we wanted to combine these metrics.

We recruited healthy participants, used an isometric intermittent grip force fatiguing paradigm, and simultaneously recorded grip force, EMG, EEG, and fMRI at 3 Tesla throughout the entire task. Participants had to generate 50% of maximum voluntary contraction (MVC) in 30 seconds blocks alternating with 30 seconds blocks of rest until exhaustion. We also measured fatigue (a subjective measure) before and immediately after completing the task. As fatigability developed, we expected to find an

increase in DI for EMG, higher EEG power in channels covering the sensorimotor areas, and increased BOLD signal in sensorimotor areas, cerebellum, and also in the insula and cingulate gyrus. We expected CMC in the beta band to increase to counter the development of fatigability and maintain isometric muscle contraction over time. As the task did not involve an isotonic motor task, we postulated that CMC in gamma would remain constant. We anticipated that EEG-informed fMRI would change as fatigability developed but have little guidance from the literature to predict the direction of effect. These results in healthy volunteers will provide new insights into the typical neuromuscular process of fatigability and, in turn, better understand fatigability in disorders. We found that with fatigability the muscles and brain increased their output to match tasks demands up to a breaking point where peak activity was reached and performance declined.

2. METHODS

2.1. Participants

We recruited 19 healthy participants (HV; 5 females, 44 ± 13 years; see Supplementary Table S1) who completed the MRI session at the National Institutes of Health (NIH). All participants were right-handed. Fifteen participants were recruited for *Post-Infectious Myalgic-Encephalomyelitis/Chronic Fatigue Syndrome project at the NIH* (NCT 02669212), and five participants were recruited for *Post-infection Convalescence of COVID-19 at NIH* (NCT 04573062). Participants were recruited via word of mouth, from referrals from the NIH Office of Patient Recruitment, and responses to study advertisements. Each participant was clinically evaluated to rule out occult illnesses and to collect research measures. Exclusion criteria included the presence of chronic fatigue, any neurological disorder outside of tension type headaches, quiescent migraines for more than 6 months, or psychiatric disorder, including depression and anxiety, and active alcohol and illicit drug use. Participants taking medication remained on their standard dosages throughout. No participants were using medications with central nervous system activity. All participants provided informed consent in accordance with the Institutional Review Board of the National Institutes of Health and the Declaration of Helsinki.

2.2. Grip force task

We used a grip force task to induce fatigability (Fig. 1A). The task was an isometric submaximal intermittent grip force task. Participants lay supine in the MRI scanner and performed repeated 30-second blocks of gripping a dynamometer (https://www.biopac.com/product/hand-clench-dynamom-for-mri/) using their dominant right hand alternating with 30-second blocks of rest. The task instructions required generating grip force at 50% of the maximum voluntary contraction (MVC). MVC was determined from the best of three brief squeezes on the dynamometer before entering the scanner. A green bar moving vertically indicated participants' force level and a static red horizontal bar indicated 50% of MVC. Tasks instructions 'Rest', 'Get Ready', and 'Go!', were presented to guide participants. The 2-second instruction ('Get Ready') was inserted at the end of each rest block to inform participants of the incoming grip blocks. All visual feedback was presented on a monitor at the foot of the MRI bore via an angled mirror in the head coil. The experimenter saw the same stimuli on a computer in the control room as well as the exact force generated by the participant. We could, thus, monitor the level of fatigability during the task. The paradigm was set for 16 blocks of grip alternating with rest in an MRI run. Most participants completed the 16 blocks but showed clear signs of fatigability, that is, their force level was well below the 50% threshold for more than one block as identified visually during the scan. A few participants (n = 3) stopped earlier than the designed 16 blocks. A few others (n = 6) did not show sign of fatigability after the first run, that is, their force level remained above or close to 50% for every block. To ensure that these participants did develop fatigability, a second MRI run was performed after resetting the task (~1 minute), up to a maximum of 32 blocks; all these participants showed signs of fatigability.

To index fatigability development, we chose eight specific blocks during the grip force task. The blocks were chosen based on each participant's performance and thus their fatigability development, rather than using blocks number. This was to ensure that we assessed fatigability at the same stage of its development. First, we defined fatigability as follows: we calculated for each block the percentage of datapoints above the required threshold of 50% of MVC. Then, we defined a block as fatigued if less than 90% of datapoints were above that threshold. Finally, to determine the onset of fatigability we looked sequentially across the fatigued blocks and chose the first block of three consecutive fatigued blocks as the onset of fatigability. We will refer to that first fatigued blocks as F_{n+1}; the *n* notation denotes that the first fatigued block differed for each participant.

We selected the eight blocks as follows. We included the 1st block and the F_{n+1} block. We also included the two following blocks to F_{n+1} to assess fatigability as it became behaviorally manifest (F_{n+2}, and F_{n+3}). We also included the block before the F_{n+1} block which represent the last

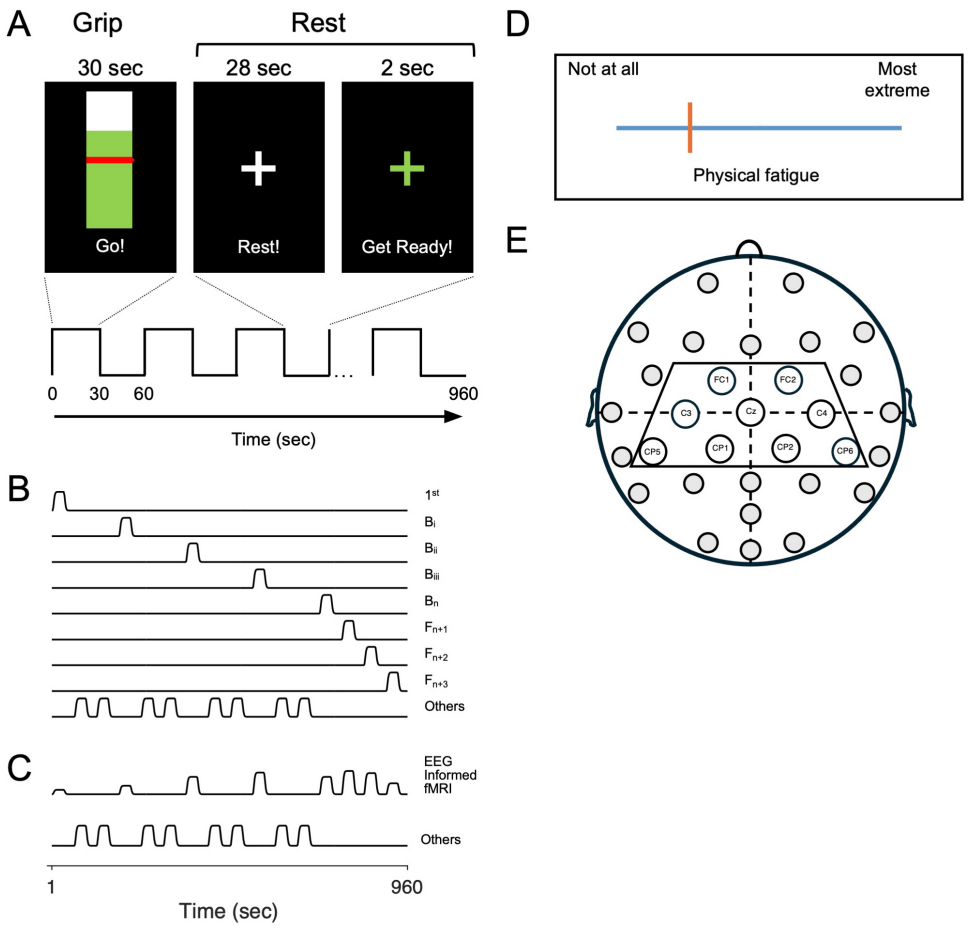

Fig. 1. (A) Task schematic. The grip force task required participants to generate force at 50% of their maximum voluntary contraction (MVC) during 30-second blocks. They used a dynamometer with their dominant right hand. The green portion indicated the participant's force level, while the static red horizontal bar indicated the 50% MVC. Blocks of 30-second grip were alternating with blocks of 30 seconds of rest (middle panel). A 2 seconds 'Get Ready!' signal appeared at the end of each rest block. (B) Hemodynamic response function (HRF). HRF for the traditional box car fMRI analysis with the eight fatigability blocks and the remaining blocks (labeled Others). (C) HRF modulated by the EEG power for the EEG-informed fMRI analysis for the eight fatigability blocks and the remaining blocks (labeled Others). First: first block; Bi, Bii, and Biii: intermediate blocks; Bn: last block before fatigability; F_{n+1}, F_{n+2}, and F_{n+3}, fatigability blocks. (D) Visual Analogue Scale (VAS) for the subjective evaluation of mental and physical fatigue before and after the grip force task. (E) EEG channels. Each circle represents one of the 31 channels recorded. The trapezoid indicates the EEG channels of interest.

successful block before fatigability onset and labeled it B_n. To allow us to track fatigability development before it became behaviorally manifest, we chose three blocks in between the 1st and B_n block (B_i, B_{ii}, and B_{iii}). We chose equidistant blocks between the 1st and B_n block, so that if B_n was 13, the B_i, B_{ii}, and B_{iii}, were 4, 7, and 10. Three $B_{i–iii}$ blocks were chosen to optimize the number of blocks collected while ensuring that all participants had $B_{i–iii}$ blocks. Thus, the 1st, B_i, B_{ii}, B_{iii}, and B_n blocks are not continuous while the B_n, F_{n+1}, F_{n+2}, and F_{n+3} blocks are continuous.

Data acquisition. We used LabView (National Instruments; www.ni.com/en-us/shop/labview.html) to present visual stimuli and recorded grip force from the dynamometer via an amplifier (MP150, BIOPAC Systems Inc.) at 100 Hz.

Data analysis. We filtered the grip force with a lowpass Butterworth of 8 Hz order of 2. We then normalized grip force to the MVC. To assess fatigability development at the group level, we measured the slopes across the average force of each block and assessed whether the average force of each block was different than the 50% MVC.

2.3. Subjective fatigue evaluation

Subjective appraisals of physical and mental fatigue were measured with visual analog scales before and after the grip force task (VAS; Fig. 1D) programmed in SuperLab (Cedrus Coorporation; www.cedrus.com/superlab). We only collected before and after data for 13 participants.

2.4. EMG

Data acquisition. We recorded EMG and EEG with BrainVision Recorder at 5 kHz (Brain Products GmbH, Gilching, Germany). We recorded EMG from the flexor and extensor carpi radialis (FCR and ECR). We placed the electrodes over the belly of each muscle, identified from palpations and testing visually the EMG response on BrainVision Recorder. We placed the ground electrode over the elbow. EMG was recorded with MRI-compatible electrodes (Ag/AgCl, laminated, carbon composition, 11 mm diameter, part EL508, BioPAC Systems, Inc.), leads (LEAD108B), connected to a BrainAmp ExG MR and via a SyncBox (https://brainvision.com/products/brainamp-exg-mr/).

Data analysis. We first removed the MRI gradient-artifact with the average artifact (AAS) method (Allen et al., 2000) as implemented in the Bergen toolbox in EEGLAB. The process of removing MRI gradient artifact affect the EMG frequency component, but removal of the artifact via our chosen method has been shown to be effective (Amador-Tejada et al., 2024). It is important to note that our analysis focuses on comparing the changes in EMG over time. Since the MRI gradient artifact has periodicity and is assumed constant in time, the MRI gradient artifacts removal would have minimal influence on our EMG analysis.

We used a bandpass filter between 20–250 Hz and removed line noise of 60 Hz, downsampled to 1000 Hz. We calculated the Dimitrov Index (DI), an EMG estimate of fatigue (Dimitrov et al., 2006; Dimitrova et al., 2005; Zhao et al., 2022). DI uses fast Fourier transform and a ratio of spectral moments -1 and 5 and considers the whole power spectrum in its computation. DI is less biased than a low/high ratio where low- and high-frequency bands are usually subjectively chosen, and DI is more sensitive than the median or mean frequency (Puce et al., 2021). We also calculated the EMG amplitude with the root-mean-square of the EMG signal (RMS); we did not rectify EMG.

To assess fatigability development, we first divided each of the eight blocks into 1 second timepoints and then calculated DI and RMS. We did not include the first 5 seconds of each block because force was at zero to start and participants had to generate considerable force to reach the 50% of MVC. Due to this instability of force generation, these timepoints are unsuitable for the analysis of time-frequency and other metrics. Note we used the same approach for the EEG, CMC, and fMRI metrics.

Since fatigability could manifest itself within or across the eight blocks (1^{st}, B_i, B_{ii}, B_{iii}, B_n, F_{n+1}, F_{n+2}, and F_{n+3}), we assessed fatigability-related changes within and across blocks. To analyze within block effects, we used robust regression to obtain the beta weights representing the rate of change (or slopes) across the 25 timepoints for each participant and then assessed significance with a *t*-test. We tested the null hypothesis that the slopes would not differ from zero. We used the robust regression implemented in Matlab with the *bisquare* weight function and a tuning constant of 4.685, which is the default. To analyze across block effects, we took the average of each of the eight blocks (i.e., all 25 timepoints) and used robust regression across the eight blocks and then assessed significance with a *t*-test. We tested the null hypothesis that the slopes did not differ from zero. We also used ANOVA to assess other potential differences among blocks using blocks as repeated measures and participants as a random factor. For the ANOVA, we tested the null hypothesis of no difference across the eight blocks. We also used this approach for EEG, CMC, and fMRI.

For statistical analyses (regression, ANOVA, and *t*-test) we used tools in Matlab and Rstudio (https://www.mathworks.com; http://www.rstudio.com/). We used the Greenhouse-Geisser correction in cases of non-sphericity as measured by the Mauchly test. We corrected for multiple comparisons with the False Discovery Rate (FDR) (Benjamini & Hochberg, 1995). We set the significant threshold *p*-value at 0.05. We used the *isoutlier* function in Matlab to remove outliers, defined as values that are more than three times the mean absolute deviations (MAD) from the median. We also included age as a covariate.

2.5. EEG

Data acquisition. We used an MRI-compatible 32-channel EEG cap (Brain Products GmbH, Gilching, Germany) with 31 EEG channels (Fp1, Fp2, F3, F4, C3, C4, P3, P4, O1, O2, F7, F8, T7, T8, P7, P8, Fz, Cz, Pz, Oz, FC1, FC2, CP1, CP2, FC5, FC6, CP5, CP6, TP9, TP10, and POz) and one ECG channel. The EEG cap was connected to a BrainAmp MR plus and a SyncBox (https://brainvision.com/products/brainamp-mr-plus/). The scalp of each participant was prepared for EEG recording by cleaning with alcohol and subsequent application of abrasive and conductive gel at each electrode location. Channels FCz was used as reference for all the electrodes, and channel AFz was used as the ground. ECG was recorded via an electrode placed on the participant's left upper back. ECG was used to remove heart-related artifact from the EEG signal.

Data analysis. We used EEGLAB to analyze the data (Delorme & Makeig, 2004). We first removed the MRI gradient-artifact with the average artifact (AAS) method (Allen et al., 2000) as implemented in the Bergen toolbox

in EEGLAB. As with EMG, removing the MRI gradient artifact affect the EEG frequency components but prior studies have reported very good concordance between EEG recorded with and without fMRI using our chosen method (Allen et al., 2000; Becker et al., 2005; Ritter et al., 2007). As stated for EMG, we are seeking changes in time which should not be affected by this analysis.

We used the FMRIB toolbox to identify and remove the ballistocardiogram artifact (https://fsl.fmrib.ox.ac.uk/eeglab/fmribplugin/). We applied a high pass filter of 0.5 Hz and downsampled to 1000 Hz. We ran Independent Component Analysis (ICA) with the *picard* algorithm (https://github.com/pierreablin/picard) and used the *iclabel* tool (https://github.com/sccn/ICLabel) in EEGLAB to automatically classify components in seven categories, including brain, muscle, eye, heart, line noise, channel noise, and other. We removed components related to muscle, eye, heart, line noise, channel noise, and other categories if the probability of a component being correctly labeled was at least 70%. We also visually inspected the data and components to further remove some components if necessary. We used the *clean_artifacts* tool to remove bad sections and bad channels using the default parameters. We interpolated the bad channels and re-referenced to the common average of all channels. We repeated the ICA and *iclabel* steps and kept only the brain components that were above 70%.

To estimate EEG power, we used the *pspectrum* tool in Matlab with the *spectrogram* option within the 0–50 Hz range and a time resolution of 1 second. This resulted in 30 timepoints per 30-second blocks. We then extracted power in frequency bands for the theta, mu, beta, and gamma bands using 4–8, 8–13, 13–30, 30–50 Hz, respectively.

We assessed fatigability development within and across each of the eight blocks as with EMG. We assessed fatigability-related changes in a subset of the EEG channels that are related to sensorimotor control (inside the trapezoid in Fig. 1E). As done with EMG, we did not include the first 5 seconds of each block.

2.6. MRI

Data acquisition. We acquired MRI data with a 3T Prisma SIEMENS scanner equipped with a 64-channel head-coil in the Nuclear Magnetic Resonance Center at NIH. First, we collected a high-resolution anatomical sagittal T1-weighted scan with TR = 2200 ms, TE = 4.25 ms, TI = 1000 ms, field of view = 100, FoV: 240 × 240 mm, matrix size: 256 × 256, flip angle = 9°, 160 slices, voxel size 1 mm^3. Then, for the grip force scans, we collected T2*-weighted EPI with TR = 2 seconds, TE = 30 ms, image matrix 64 × 64, flip angle: 70°, and FoV: 100, voxel size 3.5 mm^3. Five participants were scanned with a different protocol for the T1-weighted scan with TR = 1900 ms, TE = 3.3 ms, TI = 1100 ms, field of view = 100, FoV: 240 × 240 mm, matrix size: 256 × 256, flip angle = 7°, 176 slices, voxel size 1 mm^3 and for the T2*-weighted EPI with TR = 2.1 seconds, TE = 19 ms, multi-echo with 19, 38.21, multi-band acceleration factor of 3, and 57.42 ms echo times, image matrix 84 × 84, flip angle: 60°, FoV: 100, voxel size 2.5 mm^3.

Data analysis. We used AFNI (https://afni.nimh.nih.gov) to process anatomical and EPI data of the grip force task with the afni_proc.py tool. The EPI of the five participants with a different scanning protocol and a voxel size of 2.5 mm^3 were resampled to 3.5 mm^3 to match the other participants. The analysis included removing the first three EPI volumes, despiking the timeseries, registering the EPI data to the anatomical scan, adjusting for slice timing offsets, motion correcting the timeseries with reference to the first collected image with rigid body transformations using cubic polynomial interpolation, and spatially blurred the timeseries with a 6 mm FWHM Gaussian kernel. We applied a band-pass filter 0.01–0.1 Hz and also used @ANATICOR to remove white matter signal from the timeseries to reduce scanner-related artifacts (Jo et al., 2010). We set the motion limit at 3 mm and identified volumes with more than 10% of outliers as defined with 3dToutcount tool in AFNI in a censor file to be used subsequently in the regression analysis. The anatomical and the EPI timeseries were transformed to the MNI template with non-linear transformations.

To reveal fatigability-related brain activation for each participant, we ran multiple regression analysis with the 3dDeconvolve tool in AFNI. We formed separate regressors for each of the eight blocks (1st, B_i, B_{ii}, B_{iii}, B_n, F_{n+1}, F_{n+2}, and F_{n+3}) by convolving the onset times of each block with a square wave to form a boxcar block design. The remaining blocks were included in a separate regressor (Fig. 1B; Eq. (1)).

$$\begin{aligned}\text{BOLD} = \beta_0 + \beta_1 X_1 + \beta_2 X_2 + \beta_3 X_3 + \beta_4 X_4 + \beta_5 X_5 + \beta_6 X_6 + \\ \beta_7 X_7 + \beta_8 X_8 + \beta_{others} X_{others} + \varepsilon, \end{aligned} \quad (1)$$

where β_0 is the intercept, β_{1-8} are the estimated regressors for each individual block 1-8, β_{others} is the estimated regressor for the Others blocks, X_{1-8} are the predictors for each individual block 1–8, X_{others} is the predictor for the Others blocks, and ε is the error. An example of an HRF for one participant for each of the eight blocks (predictors X_{1-8}) is shown in Figure 1B as well as the remaining blocks (labeled *Others*; predictors X_{others}). We also included the demeaned and derivatives of head motion parameters and censored out bad volumes identified in the censor file.

At the group level, in a first analysis, we assessed movement-related activation independently of fatigability by averaging the eight estimated regressors (i.e., beta weights, β_1–β_8) for each participant and then used a *t*-test to test the null hypothesis that BOLD signal would not differ from zero. We restrained the analysis to the grey matter only with the Brainnetome atlas and SUIT cerebellar atlas (https://atlas.brainnetome.org/bnatlas.html; Diedrichsen, 2006). We thresholded the activation brain map with a $p \leq 0.001$ value as activation occurred in basically all grey matter at higher *p* values. We corrected for multiple comparisons using a cluster threshold of $p \leq 0.05$ resulting in clusters having at least 11 contiguous significant voxels; that number comes from using the residuals of the times series from the participant's regression (3dDeconvolve tool) with the AutoCorrelation Function (*ACF* option) to estimate the noise smoothness.

To assess fatigability-related activation, we used 3dLME (Chen et al., 2013) to run linear mixed-effects one-way ANOVA with all eight blocks as a repeated-measures factor and participants as a random factor. We tested the null hypothesis of no difference in BOLD signal across the eight blocks. We restrained the analysis to the grey matter only as above. We thresholded the activation brain map with a $p \leq 0.05$ and corrected for multiple comparisons using a cluster threshold of $p \leq 0.05$, resulting in clusters having at least 180 contiguous significant voxels; that number comes from using the residuals of the times series from the participant's regression (3dDeconvolve tool) with the AutoCorrelation Function (*ACF* option) to estimate the noise smoothness.

We also implemented an ROI-based analysis to complement the previous analysis within the frontal motor areas, somatosensory cortex, cerebellum, cingulate gyrus, and insula, all known to have roles in motor function and fatigue (Benwell et al., 2007; Jiang et al., 2016; Liu et al., 2002, 2003; Post et al., 2009; van Duinen et al., 2007). We used the Brainnetome atlas (https://atlas.brainnetome.org/bnatlas.html). This ROI analysis differs from the whole-brain analysis as we averaged all the voxels within an ROI and then analyzed with regression across the eight blocks. The whole-brain approach is performed on each voxel separately, and if enough significant voxels form a statistically large enough cluster, it is deemed significant. The frontal motor areas included the bilateral primary motor cortex, pre-motor, and supplementary motor areas. The cerebellum included the bilateral lobules I–IV, V, VI and dentate nucleus from the SUITE atlas (Diedrichsen, 2006). The somatosensory cortex included the bilateral area 1–3. The cingulate gyrus included the bilateral anterior cingulate sub-genual, anterior cingulate pre-genual, mid-cingulate, and post-cingulate as labeled in the Brainnetome atlas. The insula was divided in six bilateral ROIs, including the hypergranular, ventral agranular, dorsal agranular, ventral dysgranular and granular, dorsal granular, and dorsal dysgranular. We further included the temporal-parietal junction (TPJ), as in our prior work (Walitt et al., 2024) we found a significant increase for healthy volunteers compared to ME/CFS participants; 10 of the current 19 participants were healthy volunteers in that study.

2.7. Corticomuscular coherence

We assessed corticomuscular coherence (CMC) between the EEG channel C3 and the forearm muscles (ECR and FCR) in the beta and gamma bands. CMC was calculated by dividing the cross-spectrum between EMG and EEG by the auto-spectrum of EMG and EEG signal in the time–frequency domain (Liu et al., 2019). CMC indicates the linear connection between EEG and EMG and is an extension of Pearson correlation coefficient in the frequency domain. It is mathematically bounded between zero and one, with zero meaning no correlation and one meaning perfect correlation. We used the NeuroSpec2.2 (Halliday et al., 2018) toolbox (https://github.com/dmhalliday/NeuroSpec) which was used in earlier work (Beck et al., 2021; Spedden et al., 2019). The toolbox implements adaptive spectral tracking based on discrete Fourier transformations to estimate time varying CMC. The analysis builds time segments based on power of 2. We set the variable *seg_pwr* in the *sp2a2_zt* tool to 10 which resulted in 29 segments per 30-second blocks with a temporal resolution of 1.024 seconds and a frequency resolution of 0.97 Hz. Thus, for each block of 30,000 timepoints, we analyzed the first 29,696. We did not rectify EMG, in keeping with prior literature (Delcamp et al., 2023; Glories et al., 2021; McClelland et al., 2012; Neto & Christou, 2010).

We assessed fatigability development within and across each of the eight blocks in the same fashion as we did with EMG and EEG. Note that after computing CMC for each 30-second block, we removed the first four timepoints of each block to keep the same number of blocks to 25 as with EMG and EEG. To estimate the significance of CMC, we used the following equation (Amjad et al., 1997; Halliday et al., 1995): $CMCthresh = 1\text{-}p^{1/(L-1)}$, where *p* is the statistical threshold set at 0.05 and *L* is the number of segments ($L = 29$), which resulted in a value of 0.1015.

We also estimated the efferent (brain to muscles) and afferent (muscles to brain) directionality of CMC in the beta and gamma bands. We used the NeuroSpec2.11 toolbox (Halliday, 2015; Halliday et al., 2016) with the *sp2a2_R2* tool. This provides non-parametric assessment of directional coherence estimates. We used the

same analytic approach within and across each of the eight blocks.

2.8. EEG-informed fMRI

We assessed how EEG in the C3 channel could predict BOLD signal across all eight blocks with multiple regression analysis using the 3dDeconvolve tool in AFNI. We used the same regressors of the first fMRI analysis to form the HRF, corresponding to the onset times of the eight blocks, but the height of each block was further modulated by the corresponding EEG power in the theta, mu, beta, and gamma bands separately. An example of an HRF in the beta band for one participant is represented in Figure 1C (labelled *EEG-informed fMRI*). The analysis also included the remaining blocks (labeled *Others*). Thus, the timing of each block was paired with the EEG power to modulate the height of each of the boxes in the box car model, yielding an amplitude-modulated regression analysis. This provides a direct measure of the proportionality of BOLD signal related to changes in EEG power. This analysis generated one beta weight per voxel with all eight blocks pooled, unlike the previous analysis which generated one beta weight per block.

$$\text{BOLD} = \beta_0 + \beta_1 X_1 + \beta_{others} X_{others} + \varepsilon, \quad (2)$$

where β_0 is the intercept, β_1 is the estimated regressor for all eight blocks, β_{others} is the estimated regressor for the Others blocks, X_1 is the predictor for all eight blocks, X_{others} is the predictor for the Others blocks, and ε is the error. The predictors X_1 and X_{others} are shown in Figure 1C for one participant. We also included the demeaned and derivatives of head motion parameters and censored out bad volumes identified in the censor file.

At the group level, we used these EEG-sensitive regressors (i.e., beta weights β_1) in a t-test to test the null hypothesis that BOLD signal would not differ from zero. We restrained the analysis to the grey matter only. We thresholded the activation brain map with a $p \leq 0.05$ and corrected for multiple comparisons using a cluster threshold of $p \leq 0.05$ resulting in clusters having at least 190 contiguous significant voxels; that number comes from using the residuals of the times series from the participant's regression (3dDeconvolve tool) with the Auto-Correlation Function (ACF option) to estimate the noise smoothness. Because this analysis resulted in only one beta weight per participant, it is not possible to follow the changes across the eight blocks as done for all other metrics. Also note that each participant had a unique HRF since they had different EEG power profile across the eight blocks.

2.9. Associations of behavior with neuromuscular metrics

We assessed associations between behavioral measurements (grip force, VAS) and neuromuscular metrics (EMG, EEG, fMRI, CMC). We assessed whether we could explain the behavioral manifestation of fatigability (B_n block) with how the neuromuscular metrics developed during the task using regression methods. We also assessed how these neuromuscular metrics related to other blocks.

3. RESULTS

3.1. Grip force

Figure 2A shows the grip force normalized to MVC for the eight blocks (1st, B_i, B_{ii}, B_{iii}, B_n, F_{n+1}, F_{n+2}, and F_{n+3}). Participants maintained a force level at the required 50% of MVC up to B_n and started to generate less force for the remaining three blocks. The B_n block occurred at the $12.5^{th} \pm 2$ block with a ranging between the fifth and the 29^{th} block. The rate of change of the averaged force across the eight blocks decreased significantly over time ($t(18) = 6.3$, $p = 6.11.3e\text{-}06$). Further, the averaged force for the 1st, B_i, B_{ii}, B_{iii}, and B_n blocks did not differ significantly from the 50% of MVC, while the remaining three blocks (F_{n+1}, F_{n+2}, and F_{n+3}) were significantly lower than the 50% of MVC (p = 0.183, 0.669, 0.878, 0.571, 0.093, 0.0003, 0.0001, 0.0004, respectively; FDR corrected).

3.2. Subjective fatigue assessment

We collected VAS before and after the grip force task (Fig. 2B; means ± s.e.m.). Participants reported more physical fatigue after than before the task ($t(12) = 2.82$, $p = 0.02$), but no difference for mental fatigue ($t(12) = 1.36$, $p = 0.20$).

3.3. EMG

We show the Dimitrov Index (DI) of the EMG for each of the eight blocks and 25 timepoints (Fig. 3A), the slopes within each block (Fig. 3B) and the averages of each block (Fig. 3C). The thick black lines in 3A represent the robust regression fit. Fatigued muscles are expected to increase their DI values (Zhao et al., 2022). As expected, DI increased within and across each of the eight blocks (Fig. 3A). The within block effect (Fig. 3B) showed significant non-zero slopes for each of the eight blocks (all $p \leq 0.05$; FDR corrected) and no change in the slope's gradient across the eight blocks ($t(18) = 0.12$, $p = 0.90$). The average DI for each block (Fig. 3C) increased from the 1st to the F_{n+1} block and then plateaued with a slight decrease. This rise from block 1st to F_{n+1} was significant

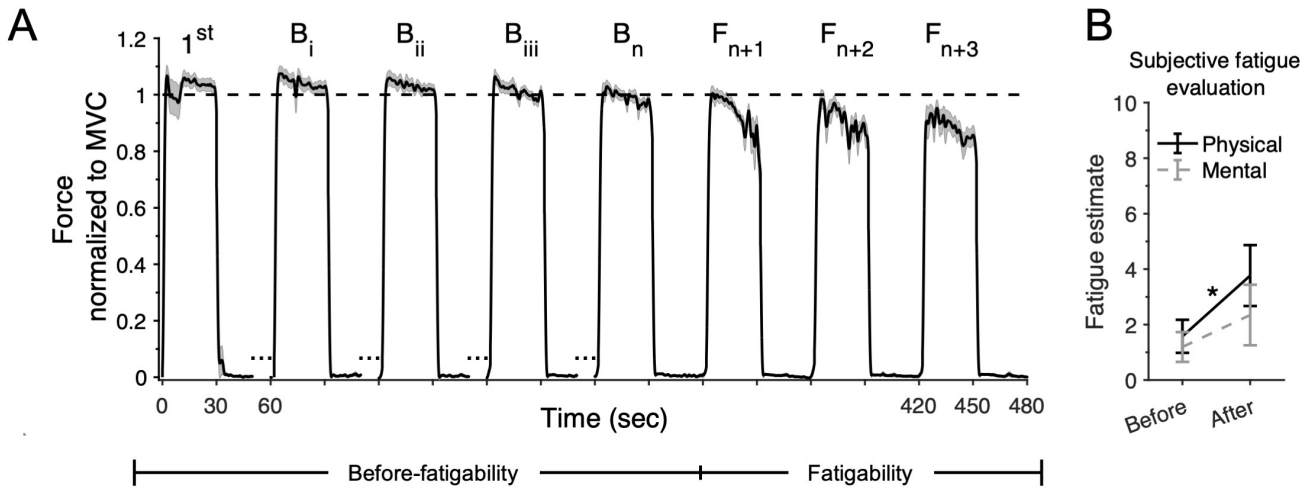

Fig. 2. Grip force and Visual Analogue Scale fatigue evaluation. (A) Grip force normalized to MVC of the eight blocks that represent fatigability development. The thick black line and shaded area indicate the group average ± s.e.m., respectively. Grip force remained leveled with the 50% of MVC up to the Bn block and then was significantly lower for the last three blocks. The three dots in between the first five blocks indicated discontinuity of those blocks. The first five blocks (1st to Bn) represented before-fatigability state, while the last three represented fatigability state (F_{n+1}, F_{n+2}, and F_{n+3}).
(B) Subjective evaluation of mental and physical fatigue before and after the grip force. Physical fatigue perception, but not mental fatigue perception, was significantly higher after than before the task.

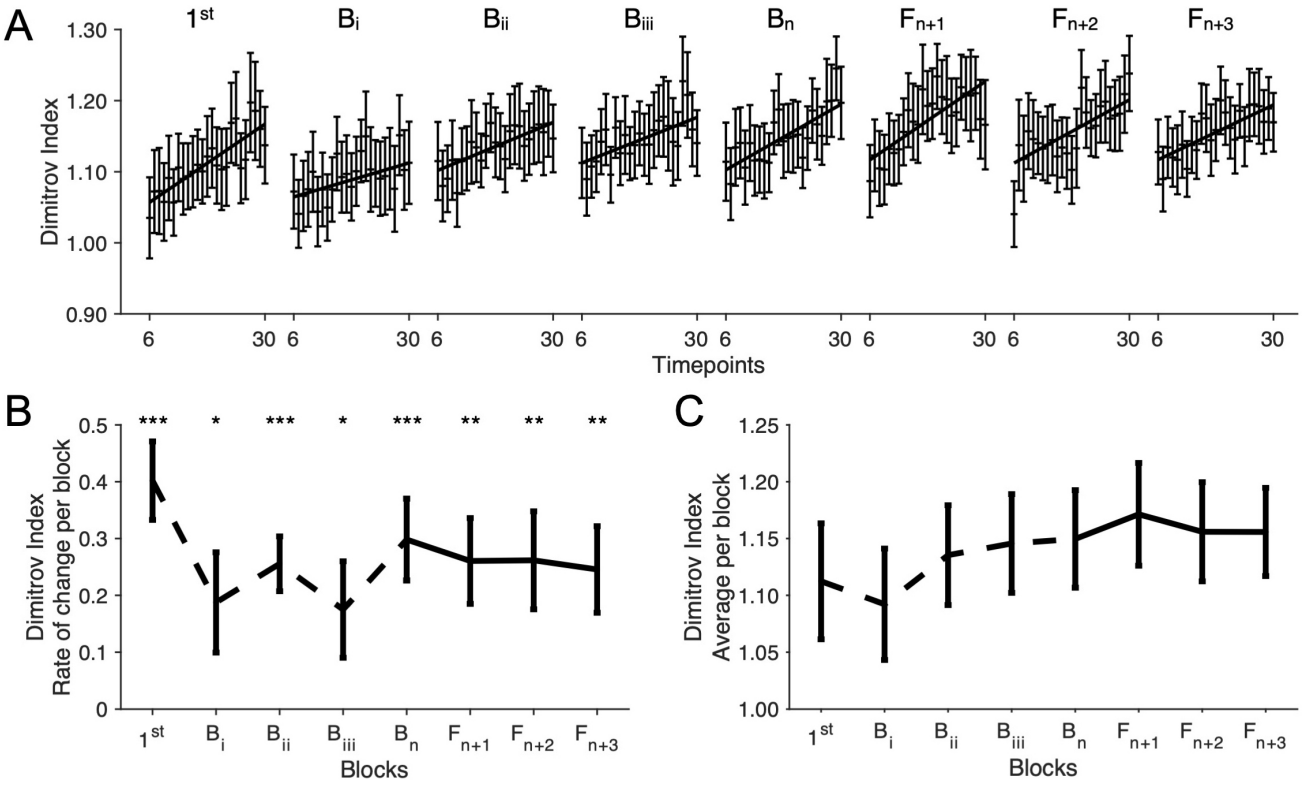

Fig. 3. EMG analyzed with the Dimitrov Index (DI) across the eight blocks. (A) DI (means ± s.e.m.) within and across all eight blocks. DI increased steadily within and across every block. (B) DI rate of change within each block (means ± s.e.m.). Rate of change for each of the eight blocks was significantly different than zero as indicated by the */**/***. (C) DI averages of each of the eight blocks. DI increased steadily and significantly across the eight blocks. *$p < 0.05$, **$p < 0.01$, ***$p < 0.001$, *ns*: not significant.

($t(18) = 2.94$, $p = 0.009$) as well as from block 1st to F_{n+3} ($t(18) = 2.84$, $p = 0.01$. There was no significant relationship of the average DI and grip force from the 1st to the F_{n+1} or F_{n+3} block that was found significant as reported above.

Concerning RMS of the EMG (Supplementary Fig. S1), the slopes within block from the 1st to F_{n+1} block were positive but not significantly different than zero (all $p > 0.09$; Supplementary Fig. S1B) and were negative for the F_{n+2} block (both $p > 0.59$). RMS amplitude (Supplementary Fig. S1C) increased from the 1st to the F_{n+1} and then plateaued with a slight decrease. This rise from block 1st to F_{n+1} was significant ($t(18) = 3.2$, $p = 0.005$) as well as from block 1st to F_{n+3} ($t(18) = 3.34$, $p = 0.004$).

Finally, we asked whether there was a relationship between the increase in DI and the increase in RMS, and a regression analysis indicated significant positive relationship (Supplementary Fig. S1D; $t(18) = 6.94$, $p < 0.0001$).

EMG demonstrated increasing muscle fatigue occurring within and across all grip blocks until fatigability occurred.

3.4. EEG

In Figure 4A–C, we display the EEG results from the C3 channel. A similar pattern of results was observed in the Cz, C4, FC1, FC2, CP1, CP2, CP5 and CP6 channels

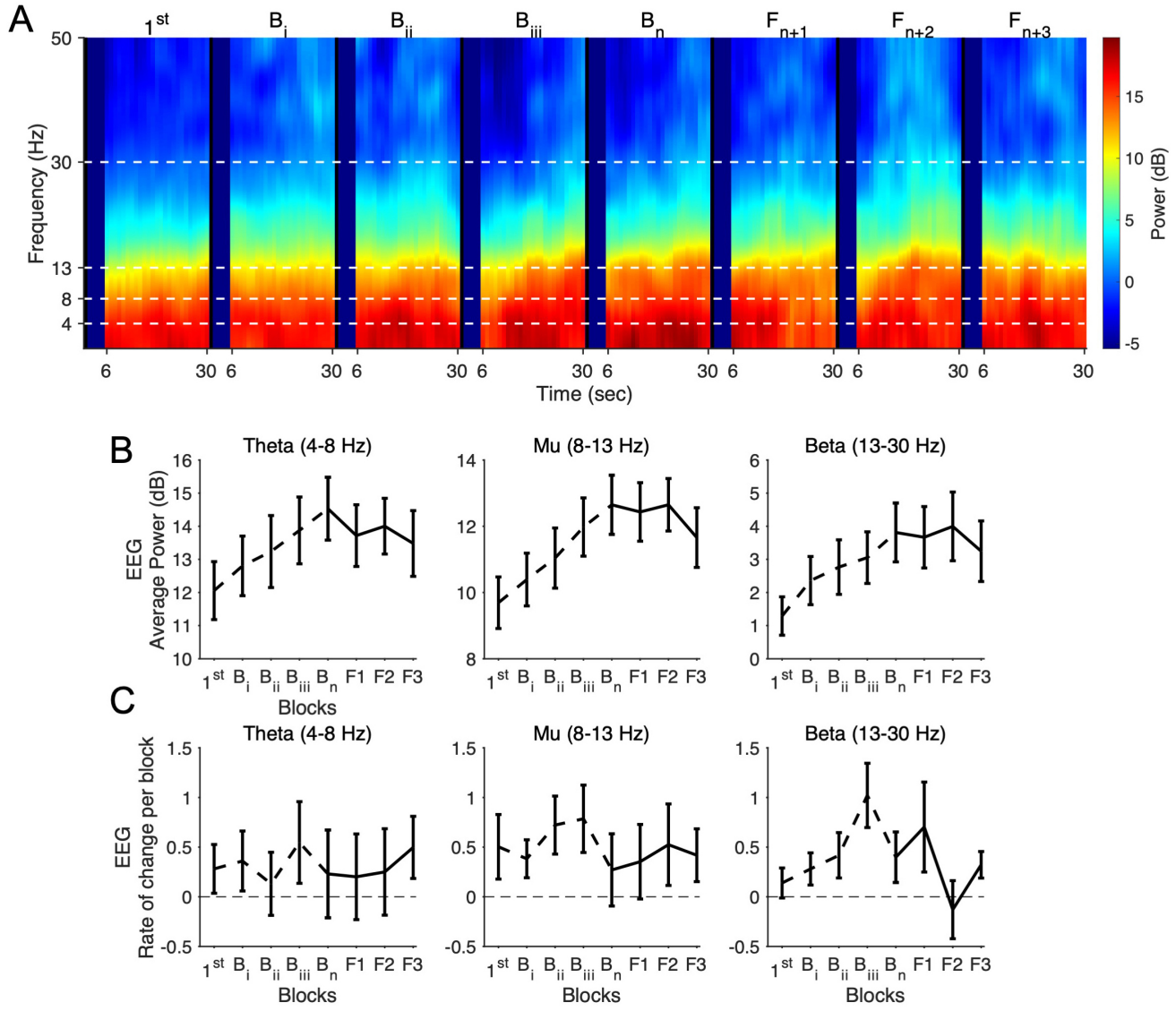

Fig. 4. EEG power in C3 channel across the eight blocks. (A) Spectrogram using Matlab *pspectrum*. The dark blue vertical bars represent the first 5 seconds of each block we omitted due to non-stationary. (B) EEG power (means ± sem) in the theta, mu and beta frequency bands. Power increased up to the Bn block and then plateaued with a slight decrease; the increase was also significant up to the F_{n+3} block. (C) Rate of change of EEG power (means ± sem) within each block. EEG power increased within block for all blocks (positive slopes). F1, F2 and, F3 are the F_{n+1}, F_{n+2}, and F_{n+3} blocks, respectively.

(see Supplementary Figs. S2–S9). The C3 channel covers the contralateral sensorimotor area and is directly involved in sensorimotor control.

The spectrogram across all eight blocks and time-points (Fig. 4A) shows that EEG power increased steadily during the first two-thirds of the task and then leveled off. This is confirmed by the block average (Fig. 4B), which increased significantly from the 1st to the B_n block in the theta, mu, and beta bans (all $p < 0.00004$) and then plateaued with a slight decrease for the last four blocks. This rise was also significant from the 1st to the F_{n+3} block for the theta, mu, and beta bands $p < 0.003$). Further, the rate of change within block (Fig. 4C) was positive for each block in the theta, mu, and beta bands (but the F_{n+2} block in beta was negative), although these were not significantly different than zero (all $p > 0.15$; $p = 0.04$ for B_{iii} in beta band). However, as can be seen in the beta band, and to a lesser degree in the mu band, power increased up to the B_{iii} block and then decreased. We assessed this rise and fall with regression which revealed a significant effect in the beta but not the mu band ($t(18) = 2.57$, $p = 0.02$ and $t(18) = 1.21$, $p = 0.29$).

Further, the rate of change within block (Fig. 4C) was positive for each block in the theta, mu, and beta bands (but the F_{n+2} block in beta was negative), although these were not significantly different than zero (all $p > 0.15$; $p = 0.04$ for B_{iii} in beta band). However, as can be seen in the beta band, and to a lesser degree in the mu band, power increased up to the B_{iii} block and then decreased. We assessed this rise and fall with regression which revealed a significant effect in the beta but not the mu band ($t(18) = 2.57$, $p = 0.02$ and $t(18) = 1.21$, $p = 0.29$).

Thus, in the early phase of the task, before fatigability is behaviorally measurable, EEG power increased from block to block as well as within each block. Immediately before fatigability became manifest behaviorally, EEG power reached a plateau and the rate of change within blocks decreased afterwards.

3.5. fMRI

In the first analysis, we assessed movement-related activation independently of fatigability by averaging all eight blocks. As expected, we found significant activation (Supplementary Fig. S10A) bilaterally in the motor network including primary motor cortex, somatosensory cortex, pre-motor, supplementary motor areas, cingulate cortex, putamen, cerebellum, parietal areas but also in the insula, dorsal-lateral pre-frontal cortex, thalamus, and temporal cortex. This activation observed across most of the brain indicates that the task was quite challenging and engaged most of the brain.

To find fatigability-related activation, we used one-way ANOVA across the eight blocks. We found one large cluster covering the superior and inferior posterior brain (Fig. 5A). To assess regional differences within this large cluster, we divided the cluster into four distinct regions using AFNI's 3dExtrema to identify the voxels with maximum values and created four ROIs of 19 voxels, centered on these voxels. These ROI were the left precuneus (x-5, y-67, z48), left lingual gyrus (x-9, y-68, z1), and left and right cerebellum (lobule VI; x-18, y-62, z-21 and x21, y-64, z-20). In these ROIs, BOLD significantly increased up to the B_n block (Fig. 5B–C; all $p \leq 0.02$) and then decreased; note that in the lingual gyrus BOLD decreased only at the F_{n+2} block. The rise was also significant from the 1st to the F_{n+3} block (all $p \leq 0.018$). We did not find any significant difference between the two scanning protocols.

We complemented this analysis with an ROI approach. We selected ROIs that were shown to be involved with fatigability (Benwell et al., 2007; Jiang et al., 2016; Liu et al., 2003; Post et al., 2009; van Duinen et al., 2007) but in which we did not find fatigability effects. Those included the bilateral primary motor cortex (M1), pre-motor, supplementary motor area (SMA), somatosensory cortex, cingulate gyrus, and insula (Fig. 5D shows M1, pre-motor, SMA, and somatosensory cortex). We also added the right TPJ identified in our prior work (Supplementary Fig. S10B) (Walitt et al., 2024). We found that BOLD in the left M1, pre-motor, and somatosensory cortex was high and did not change across blocks ($p = 0.66$, 0.55, and 0.15; Fig. 5E–G) whereas in the right hemisphere BOLD was initially low and increased steadily ($p = 0.05$, 0.002, and 0.003) but did not reach the same level of activation as the ROIs in the left hemisphere. In the SMA bilaterally (Fig. 5H), BOLD remained high for all blocks and did not change across blocks much like the left M1. In the right TPJ cluster identified in our prior work (Walitt et al., 2024), we found a significant increase of BOLD across the eight blocks ($p = 0.01$; Supplementary Fig. S10B, C). In the cingulate gyrus and insula, there were no significant changes across blocks.

3.6. Corticomuscular coherence

CMC amplitude. We assessed corticomuscular coherence (CMC) between C3 and forearm muscles in the beta and gamma bands (Fig. 6). CMC in the beta band increased within each of the eight blocks (Fig. 6A) as shown by the positive slopes (the thick black lines represent the robust regression fit). The slopes for each block except the 1st block were significantly greater than zero (Fig. 6B; all $p \leq 0.05$, $p = 0.25$ for the 1st). Also, the gradient of the slopes increased across the eight blocks, mostly between the 1st and B_i, block, but slightly failed to reach the significant statistical threshold ($t(18) = 2.02$,

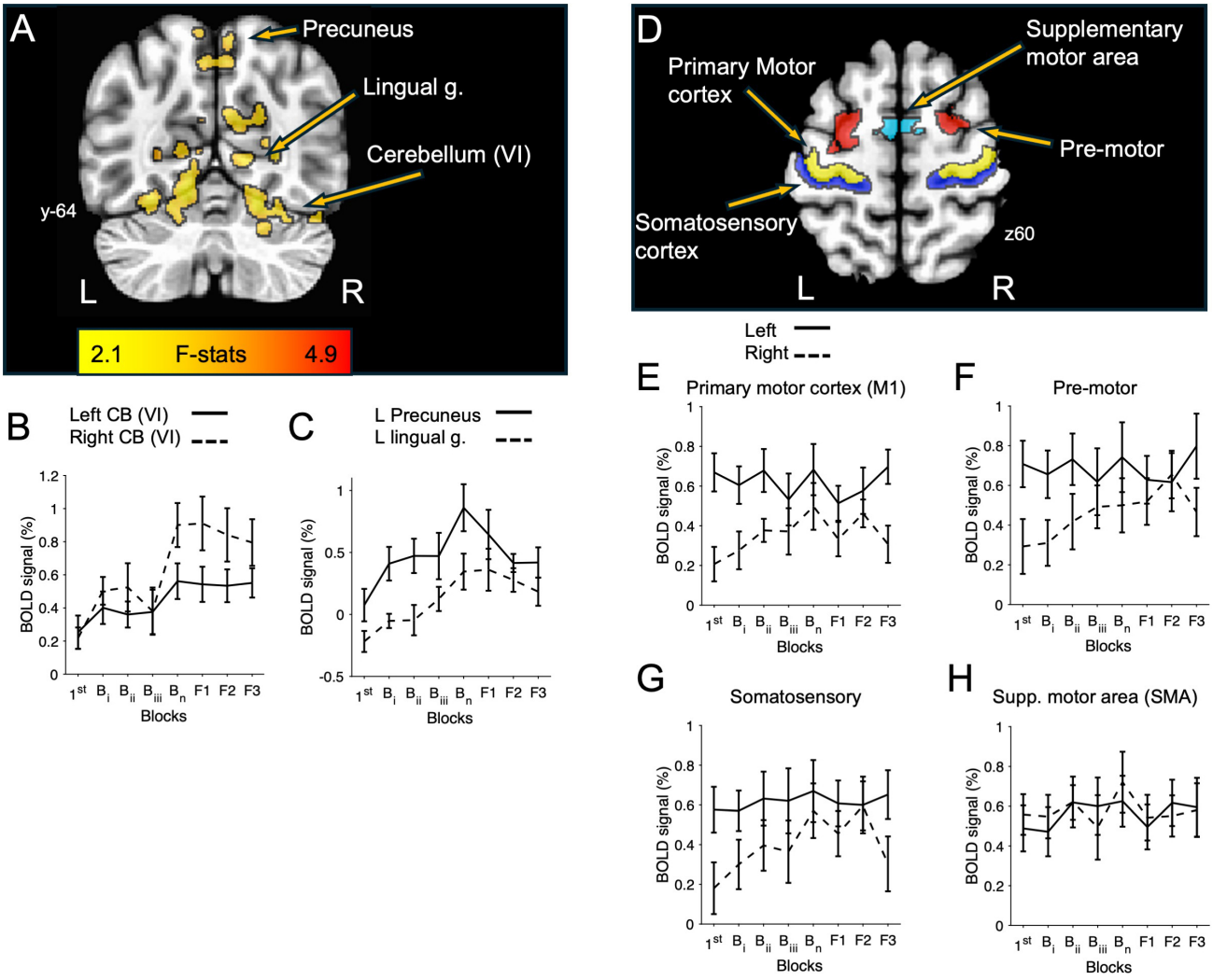

Fig. 5. fMRI across the eight blocks. (A) Whole-brain analysis with one-way ANOVA revealed a large cluster in the posterior brain. Color represents the *F* statistic of the ANOVA. (B, C) BOLD signal. The large cluster in *A* was broken in four separate regions: precuneus, lingual gyrus, and bilateral cerebellum lobule VI. BOLD signal (means ± s.e.m.) increased significantly for all four regions. (D–H) ROI analysis. (D) ROI included the bilateral primary motor cortex (M1), pre-motor, supplementary motor area (SMA), and somatosensory cortex. (E–H) BOLD signal across the eight blocks. *L*: left, *R*: right, *g*: gyrus. F1, F2 and, F3 are the F_{n+1}, F_{n+2}, and F_{n+3} blocks, respectively.

p = 0.06). Regarding the average CMC amplitude for each block (Fig. 6C), it remained stable across all blocks (one-way ANOVA, $F(7, 126) = 0.66$, $p = 0.70$). CMC was significantly higher than the estimated *CMCthresh* of 0.1015 for each block (*t*-test for each block, $t(18) > 6.18$, $p < 0.001$, FDR). Since we removed the first four timepoints, we also analyzed the results with $L = 25$ giving a *CMCthresh* of 0.1173. This also revealed that each block was significantly higher than this threshold ($t(18) > 4.25$, $p < 0.001$, FDR). Also, as can be seen in Figure 6A, the last timepoint for a few blocks was much higher than the previous timepoints; note these did not meet the criteria of outliers as being three times the MAD from the median. We also used robust regression to minimize the effects of those irregular timepoints. To further address this, we ran the same analysis without the last timepoints for each block, and we found the same effects for the slopes in each block (all $p \leq 0.05$, but not the 1st) with no change across blocks for the average.

Next, we asked whether CMC could predict some behavioral metrics. We found a significant and positive relationship (Fig. 6D) between the average of the CMC slopes from block 1st to B_n and the number of blocks performed when B_n was reached ($F(1, 17) = 6.06$, $p = 0.03$).

CMC in gamma band resulted in a very similar pattern of results as noted with the beta band (Supplementary Fig. S12). That is, CMC increased significantly within blocks and the amplitude of each block averages remained stable across blocks. However, the relationship with the last successful block (B_n) was not significant for

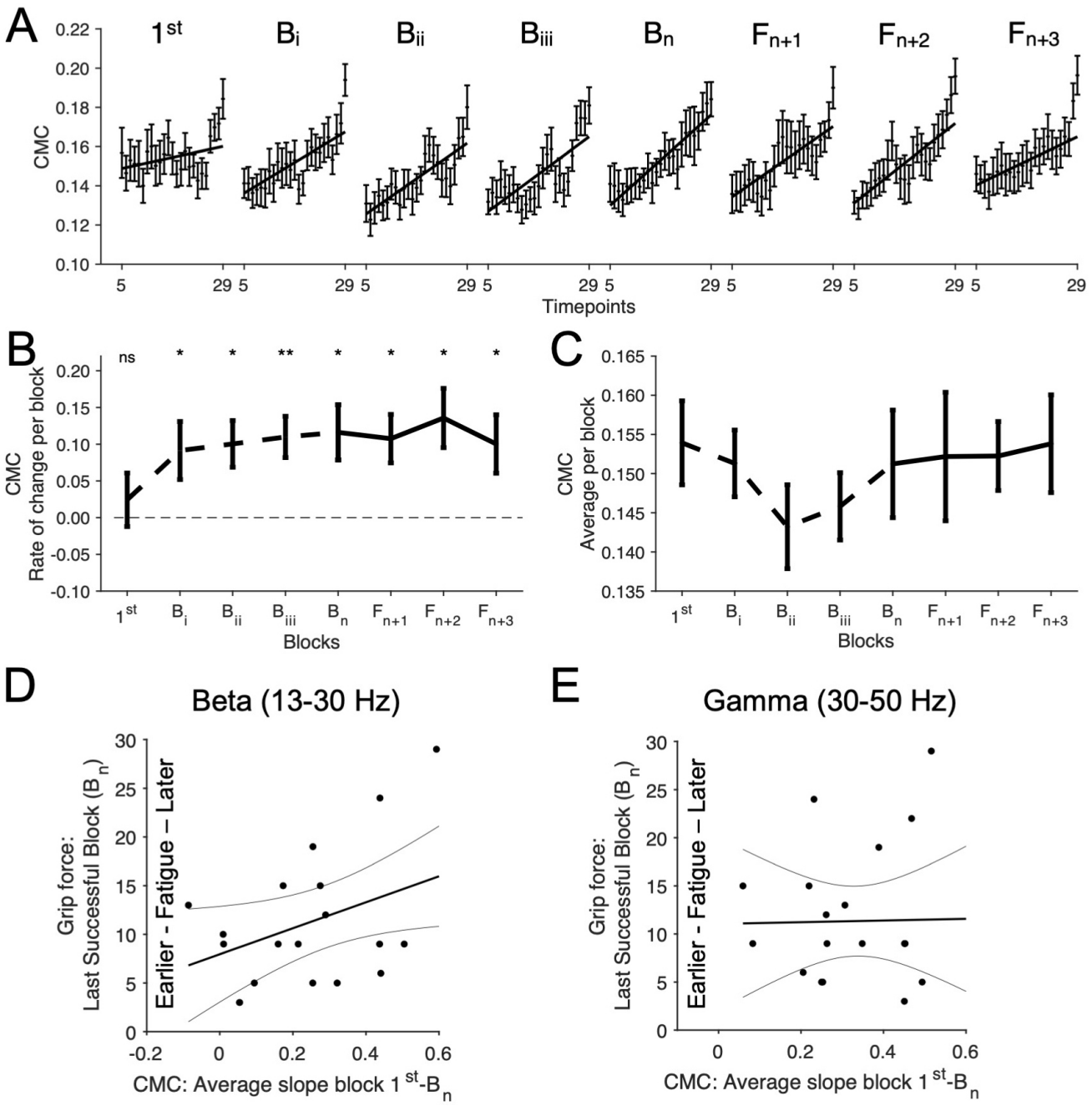

Fig. 6. Corticomuscular coherence (CMC) in the beta band (13–30 Hz) between C3 and forearm muscles across the eight blocks. (A) CMC (means ± s.e.m.) within and across all eight blocks. CMC increased steadily within every block but not across blocks. (B) CMC rate of change within each block (means ± s.e.m.) always increased and was significant for seven out eight blocks, as indicated by the */**/***. (C) CMC averages of each of the eight blocks did not change significantly across the eight blocks. (D) In the beta band, higher CMC was associated with later occurrence of the Bn block, that is, the last block before fatigability. (E) In the gamma band, higher CMC was not associated with the occurrence of the Bn block. *$p < 0.05$, **$p < 0.01$, ***$p < 0.001$, *ns*: not significant.

the slope's averages as it was for the beta band (Fig. 6E; $F(1, 17) = 0.006$, $p = 0.94$).

Thus, CMC increased with fatigability in the beta and gamma bands, but this increase was related to the delayed onset of fatigability only in the beta band.

CMC directionality. We also assessed directionality of CMC in the beta and gamma bands (Fig. 7). In the beta band for the efferent direction (brain to muscles; Fig. 7A–C), no slopes were significantly different than zero (Fig. 7B; all $p > 0.37$, FDR) and there were no significant changes in the slopes across blocks (one-way ANOVA $F(7, 126) = 0.55$, $p = 0.79$). However, the amplitude of the CMC beta Fig. 7C) increased significantly from the 1st to the B_n block ($t(18) = 2.52$, $p = 0.02$), but failed to reach the

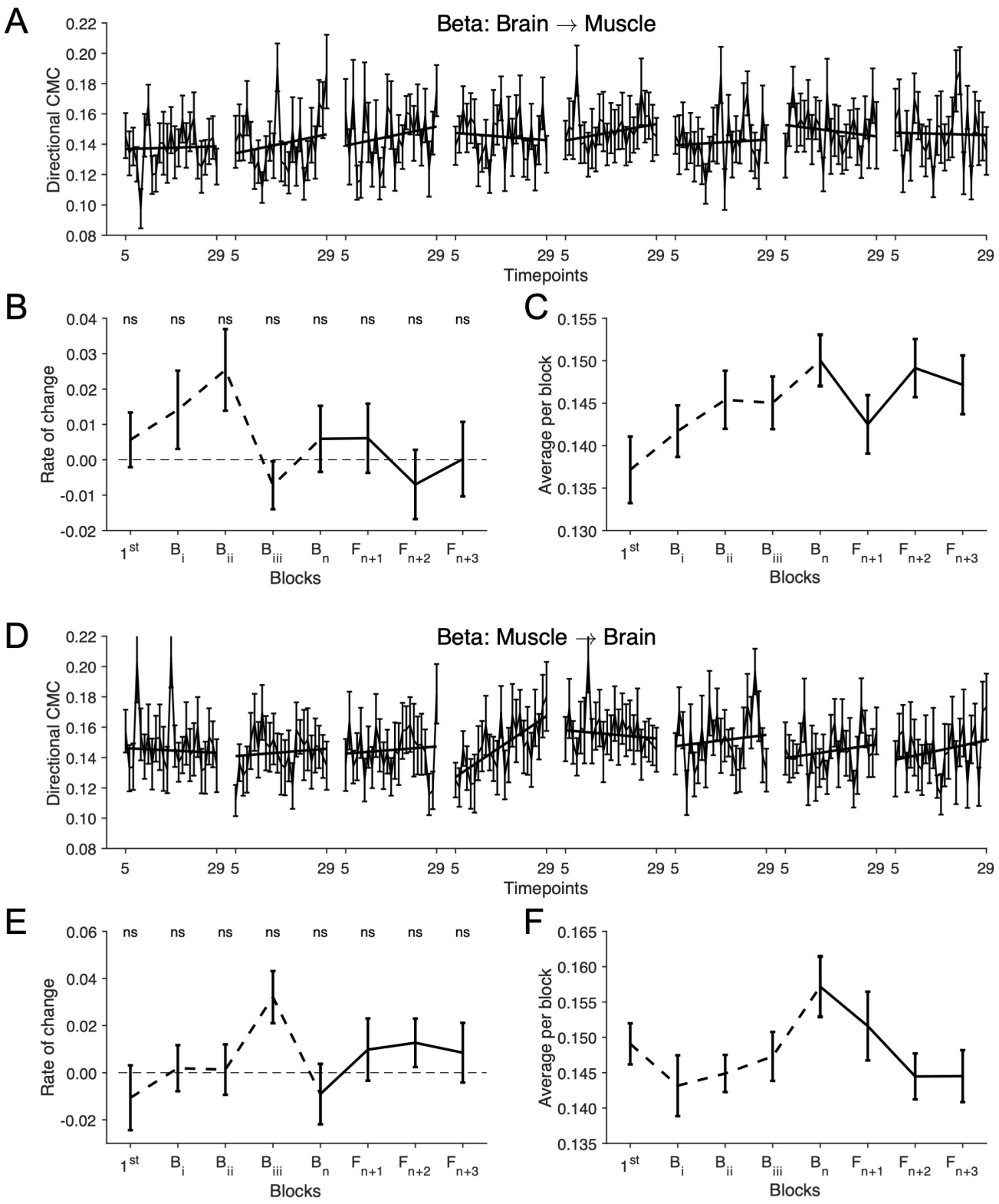

Fig. 7. CMC Directionality component in the efferent (brain to muscles) and afferent direction (muscles to brain) in the beta and gamma bands. (A–C) In the beta band, the average efferent direction component of each block increased across blocks. (D–F) In the beta band, the average afferent direction component increased up to the B_n block and then decreased significantly. (G–I) In the gamma band, the efferent direction component did not change significantly within or across blocks. (J–L) In the gamma band, the average afferent direction component increased from the 1st to the F_{n+1} block. *ns*: not significant.

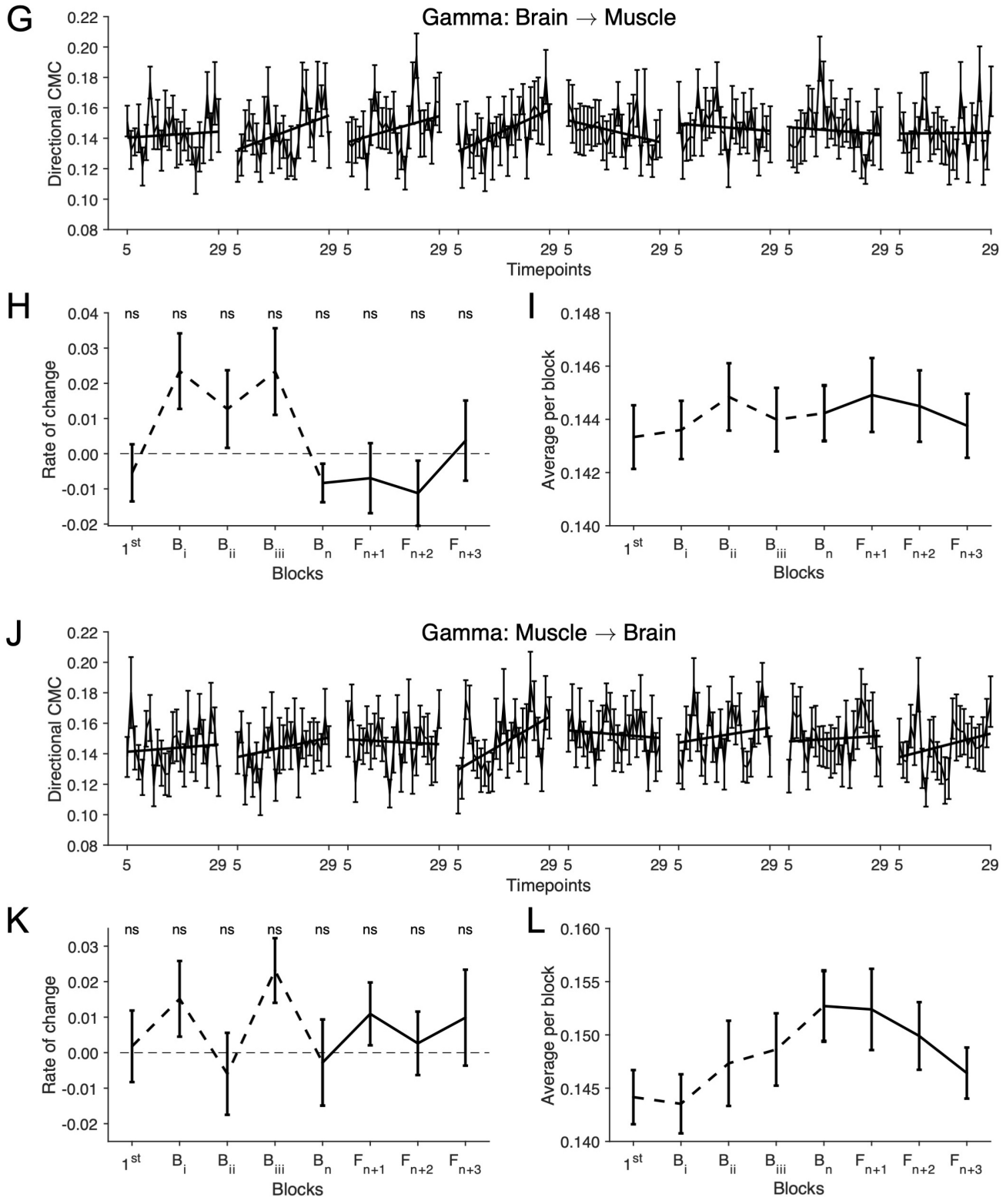

Fig. 7 (*Continued*)

statistically significant threshold from 1st to F_{n+3} block and $t(18) = 1.99$, $p = 0.06$). In the beta band for afferent direction (muscles to brain; Fig. 7D–F), no slopes were significantly different than zero (Fig. 7E; all $p > 0.12$, FDR) and there were no significant changes in the slopes across blocks (one-way ANOVA $F(7, 126) = 1.16$, $p = 0.33$). For the amplitude (Fig. 7F), the one-way ANOVA was not significant ($F(7, 126) = 1.72$, $p = 0.11$). However, directional CMC (Fig. 7F) increased across the first five blocks (1st to B_n block) and then steadily decreased from B_n to F_{n+3}. We tested whether this rise and fall were different. We separately estimated the rise and fall with linear robust regression for each participant and tested the null hypothesis of no difference between the rise and fall with *t*-test. This resulted in a significant difference between the rise and fall ($t(18) = 2.47$, $p = 0.02$).

In the gamma band for efferent direction (brain to muscles; Fig. 7G–I), no slopes were significantly different than zero (Fig. 7H; all $p > 0.30$, FDR) and there were no significant changes in the slopes across blocks (one-way ANOVA $F(7, 126) = 2.19$, $p = 0.06$ after Greenhouse-Geiser correction). For the amplitude (Fig. 7I), the one-way ANOVA was not significant ($F(7, 126) = 0.24$, $p = 0.97$). In the gamma band for afferent direction (muscles to brain; Fig. 7J–L), no slopes were significantly different than zero (Fig. 7K; all $p > 0.16$, FDR) and there were no significant changes in the slopes across blocks (one-way ANOVA $F(7, 126) = 1.03$, $p = 0.41$). However, the amplitude of the CMC gamma increased significantly across blocks from 1st to F_{n+3} (Fig. 7L; $t(18) = 2.20$, $p = 0.04$).

Thus, beta CMC was observed to change with fatigability in both the afferent and efferent directions while gamma CMC only changed in the efferent direction. We found no significant correlation for any of the CMC directionality metrics with behavior.

3.7. EEG-informed fMRI

We assessed how EEG could inform BOLD signal in the theta, mu, beta, and gamma bands (Fig. 8) with an HRF

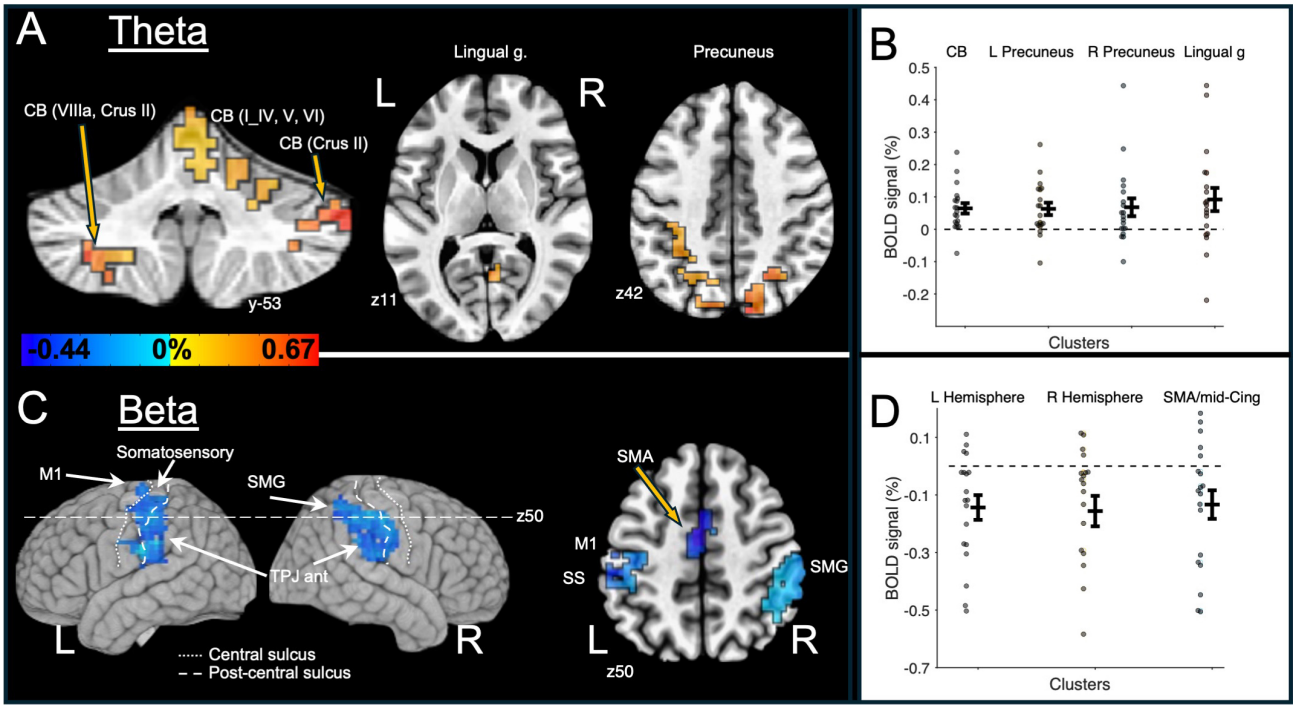

Fig. 8. EEG-informed fMRI between the C3 channel and BOLD signal for the eight blocks in the theta and beta bands. Color represents the group average of the EEG-fMRI association, that is, beta weights of the regression. (A) Theta band. A cluster was in the posterior brain straddling the precuneus, cuneus, and lingual gyrus, another in the right cerebellum (lobule I–IV, V, and VI and right Crus II), and another in the left cerebellum (lobule VIIIa and Crus II). (B) Regression coefficients for the theta clusters. Each dot represents one participant and the mean ± s.e.m. is shown. (C) Beta band. Clusters in the left sensorimotor areas (SM) straddling the primary motor cortex (M1) and somatosensory cortex (SS), bilateral anterior portion of the temporal-parietal junction (TPJ), supramarginal gyrus (SMG), SMA, and mid-cingulate gyrus. The dashed horizontal white line is set at z50 like the axial slice. The central and post-central sulcus were carefully drawn by hand but are approximate. (D) Regression coefficients for the beta clusters; for details see (C). *L*: left, *R*: right, *g*: gyrus., *M1*: primary motor cortex; *SS*: somatosensory cortex, *CB*: cerebellum, *SMG*: supramarginal gyrus, *SMA*: supplementary motor areas. *TPJ*: temporal-parietal junction.

Table 1. Brain areas with significant EEG-informed fMRI in the theta band

	MNI coordinates			Cluster volume	*t* values	
Brain areas	x	y	z	mm³	Mean	Max
L/R Cerebellum lob. I–IV, V, VI, crus II	9	-65	-25	432	2.58	5.82
L Lingual gyrus/ precuneus	-10	-74	31	296	4.89	7.66

MNI coordinates of brain areas with significant group main effects in the theta band. *L*: left, *R*: right; lob: lobule.

Table 2. Brain areas with significant EEG-informed fMRI in the beta band

	MNI coordinates			Cluster volume	*t* values	
Brain areas	x	y	z	mm³	Mean	Max
R SMG/TPJ	56	-29	37	310	-2.53	-4.15
L Sensorimotor/TPJ	-51	-26	43	270	-5.05	-8.13
L SMA/mid-cingulate	-1	-5	49	146	-7.23	-10.2

MNI coordinates of brain areas with significant group main effects in the beta band *L*: left, *R*: right; *SMG*: supramarginal gyrus, *SMA*: supplementary motor area. *TPJ*: temporal-parietal junction.

modulated by the EEG power. First, we evaluated whether the polarity of the EEG-fMRI association differed across different frequency bands (Goldman et al., 2002; Kilner et al., 2005; Laufs et al., 2003; Scheeringa et al., 2016). We found, without any statistical thresholding, that the percentage of voxels with a positive association for each of the theta, mu, beta, and gamma bands were 81.3%, 53.3%, 16.8%, and 25.9%, respectively. Accordingly, after statistical thresholding, we found clusters with positive association in the theta bands, but clusters with negative association in the beta band; we found no cluster in the mu or gamma band. We show these clusters in Figure 8A–C and each participant's BOLD signal and the group mean ± s.e.m. in Figure 8B–D; these represent the coefficients of the regression analysis done with the model in Figure 1C. As explained in the *Methods,* this regression analysis produces only one regressor per participant, so we cannot plot the coefficients across blocks like in Figure 5.

In the theta band (Fig. 8A, B; Table 1), we found a cluster in the posterior brain straddling the precuneus, cuneus, and lingual gyrus, a cluster in the right cerebellum (lobule I–IV, V, and VI and right Crus II), that also included the left cerebellum (lobule VIIIa and Crus II). We show each participant beta weight of the regression in Figure 8B after dividing the cluster in the posterior brain into a left, right precuneus, and lingual gyrus clusters. Also, BOLD signal for each cluster, as obtained with the regression in which the eight blocks were individually analyzed (Fig. 1B; Eq. (1)), increased significantly across the eight blocks (Supplementary Fig. S11A; all $p < 0.008$). These three clusters overlapped slightly with the one found in the first fMRI analysis (Fig. 5). For the cluster in the precuneus, cuneus, and lingual gyrus the overlap was 57 voxels; for the cluster in the right cerebellum the overlap was 18 voxels and two voxels in the left cerebellum. Thus, these three current clusters and the one in Figure 5 only slightly overlapped but were contiguous, spanning the same regions.

In the beta band (Fig. 8C; Table 2), there was a cluster in the left hemisphere straddling the primary motor cortex, somatosensory cortex, and the anterior portion of the TPJ (Igelström & Graziano, 2017). We also found a cluster in the right hemisphere spanning the supramarginal gyrus and anterior portion of the TPJ; note that the cluster did not overlap with the one we found in our prior work which was more posterior (Supplementary Fig. S10B) (Walitt et al., 2024). We also found a smaller cluster in the SMA and mid-cingulate gyrus (BA 24). BOLD signal for each cluster, as obtained with the regression in which the eight blocks were individually analyzed (Fig. 1B; Eq. (1)), decreased across the eight blocks, but not significantly (Supplementary Fig. S11B; all $p > 0.74$).

Thus, EEG-informed MRI, in which we use an EEG-modulated HRF, identified different brain areas that were not revealed with a more conventional fMRI analysis.

4. DISCUSSION

We studied how the neuromuscular system changes and adapts during fatigability development using multimodal neuroimaging and neurophysiology with an isometric intermittent grip force task in healthy participants. We selected specific portions of the grip force task for each participant to assess fatigability development as it occurred. Our neuroimaging and neurophysiology data showed a steady stream of changes before fatigability was manifest behaviorally. Our most novel results relate to the changes in CMC and EEG-informed fMRI. We first discuss the EMG and EEG separately and then their combined effects with CMC, then we discuss the BOLD and then its combined effects with EEG, that is, EEG-informed fMRI.

4.1. EMG

Regarding EMG, as expected we found a steady increase within and across blocks of the Dimitrov Index (DI) as reported before (Dimitrov et al., 2006; Dimitrova et al., 2005; Puce et al., 2021; Zhao et al., 2022) and we also

found an increase of EMG amplitude across blocks (Sun et al., 2022). The DI is a time-frequency metric with a low/high ratio of the EMG power spectrum which captures the decline in muscles fiber conduction velocity (MFCV) that accompanies fatigability, also referred to as reduced action potentials velocity (Bigland-Ritchie et al., 1981; Piper, 1912; Wan et al., 2017). The DI increase is, thus, indicative of muscle fatigability. This fatigability-related reduction in MFCV can be caused by several factors, including reduced central drive, reduced motoneurons firing, and the accumulation and depletion of various metabolites inside the muscles (Taylor et al., 2016; Wan et al., 2017). The amplitude increase of EMG comes from the recruitment of more motor units and the increase of motor units firing rates which are features of fatigability (Merletti et al., 2010; Sun et al., 2022). These data indicated the presence of peripheral fatigue.

4.2. EEG

We found that EEG increased steadily in all frequency bands and in various channels from the 1st block up to the B_n block, that is, the last block before fatigability onset, and then plateaued with a slight decrease. Prior work on EEG also reported fatigability-related increase of EEG (Berchicci et al., 2013; Enders et al., 2016; Guo et al., 2014; Johnston et al., 2001; Schillings et al., 2006; Suviseshamuthu et al., 2022; Wang et al., 2017). Here, we show changes during the fatigability development with a much higher temporal resolution of 1 second. Further, these changes in EEG preceded fatigability onset, that is, the B_n block. We found these effects in a host of channels contralateral but also ipsilateral, for example, C3, Cz, C4, FC1, and FC2 that correspond to brain areas likely including the primary motor cortex, pre-motor, supplementary motor area, and somatosensory cortex as well as subcortical areas that are involved in all aspects of sensorimotor control. Increases in EEG power can be interpreted as increase in neuronal activity synchrony (Nunez & Srinivasan, 2006). This increase in EEG power over the C3 channel and others might indicate that the brain was recruiting more motor units and/or increasing the firing rate of the already active motor units, due to changes inside the muscles that were reducing the MFCV. This recruitment would seem to become more synchronized as fatigability developed.

It might appear unexpected to find strong activity in the ipsilateral channels, for example, in C4. But a prior EEG study showed that the center of brain activity changed as fatigue developed, with more involvement of the ipsilateral hemisphere (Liu et al., 2007). They proposed that this shift was to recruit different unfatigued portion of the brain to maintain optimal performance. This ipsilateral involvement likely used the ipsilateral projections (Dum & Strick, 1996).

Thus, as fatigability developed more and more of the brain activity was devoted to performing the task.

4.3. Corticomuscular coherence

We found increasing CMC as fatigability developed in the beta and in the gamma bands. Those changes occurred within blocks, as CMC increased within each block, although not significantly for the 1st block. The fact that the CMC slope in the 1st block was not significantly different than zero but became so afterward suggests that changes also occurred across blocks, albeit to a lesser degree. The CMC amplitude (averaged per block) did not vary significantly across blocks (Fig. 6C). This null result across blocks most likely relates to the 30-second rest in between each grip block which may have allowed enough time for the neuromuscular system to recover to some extent. Also, in the beta band, but not the gamma band, we found that the increasing CMC within block was related to delayed fatigability onset (Fig. 6D, E), as participants who showed higher CMC fatigued less quickly. This suggests that increasing CMC in the beta band, but not in the gamma band, was an effective adaptive neuromuscular process to slow fatigability and maintain performance to match the task instructions. This fatigability-related beta band increase also echoes work showing that increased CMC in the beta range improved motor performance during a steady motor task (Kristeva et al., 2007; Mendez-Balbuena et al., 2013; Omlor et al., 2011).

We also analyzed the efferent and afferent component of CMC as the correlative nature of the CMC computations did not allow to disentangle its directionality. Our analysis of CMC directionality revealed that in the beta band, efferent CMC (brain to muscles) increased steadily across blocks up to the B_n block, that is, the last block before fatigability, and then plateaued, while afferent CMC (muscles to brain) increased up to the B_n block and then dropped abruptly. In the gamma band, the afferent CMC increased steadily up to the F_{n+1} block, although the CMC values at the F_{n+1} block were basically similar to those of the B_n block. Thus, afferent gamma CMC resembled the afferent beta CMC, but with a less abrupt change.

Only one prior study assessed CMC directionality of fatigability, but they measured CMC before and after a sustained fatiguing task (Liang et al., 2021). They reported more beta band efferent CMC before the task but more beta and gamma bands afferent CMC after the task. Thus, despite using different experimental design, task, and analysis, both studies found afferent increase in the

beta and gamma bands with fatigability. But our methods allowed us to follow CMC during fatigability development at a high temporal resolution of 1 second.

This increase of efferent and afferent beta CMC up to their peak at the B_n block likely indicates increased synchronous and rhythmic activity between the brain and muscles to meet the task demands and delay or counter the development of fatigability. The leveling off and decrease of efferent and afferent beta CMC, respectively, from the B_n block until the end of the task likely indicate a break down or inefficiency in the rhythmic interaction between the brain and muscles due to fatigability which could have impaired performance. A similar process could explain the afferent gamma CMC.

This process likely implicates the muscles afferent feedback via the Ia muscle fibers and the group III/IV fibers. During fatiguing exercise, muscles spindles can reduce their firing rate which reduces group Ia muscle afferents firing rate which, in turn, inhibit spinal motoneurons output (Taylor et al., 2016). The group III/IV sensory fibers carry information about the mechanical and biochemical properties of the muscles and relay that information to the motoneurons in the spinal cord but also to the brain (Amann et al., 2020; Laurin et al., 2015). On the one hand, these fibers can increase muscle blood flow and oxygenation and delay fatigability. On the other hand, they can reduce the central motor drive via spinal and supraspinal inhibition (Amann et al., 2011, 2013) and can inhibit M1 (Sidhu et al., 2017, 2018). Thus, during exercise the group III/IV sensory fibers can induce central fatigability by exerting inhibitory influences on central motor drive. The plateau of beta band efferent CMC at the B_n block, as well as the EEG plateau at B_n, might be a consequence of the afferent CMC input to the brain via the group III/IV fibers. Support for this hypothesis that afferent feedback caused central fatigability also comes from the fact the EMG showed signs of fatigability earlier than EEG as we found increased DI within each block starting at the 1st block, whereas in EEG we found changes mostly across blocks and the changes within blocks occurred after the 1st block. Thus, the brain and muscles increased their interaction up to a point before fatigability emerged and then decreased their communication as fatigability became more manifest.

4.4. fMRI

We found fatigability-related BOLD changes in the precuneus, lingual gyrus, and cerebellum and these showed an increase across the eight blocks. Our ROI analysis also showed that BOLD increased across blocks in the ipsilateral M1, somatosensory cortex, and pre-motor cortex while in the contralateral hemisphere BOLD was high from the onset of the task and remained high throughout. We found no area with a BOLD decrease across blocks. Prior work also reported increased BOLD during fatiguing tasks in various brain areas (Benwell et al., 2007; Jiang et al., 2016; Liu et al., 2002, 2003; Post et al., 2009; van Duinen et al., 2007). This BOLD increase indicates enhanced neuronal activity (Logothetis, 2008) as fatigability developed.

The precuneus and lingual gyrus are involved in visual processing and visual and spatial attention (Cavanna & Trimble, 2006), and the BOLD changes in these areas could relate to the attention demands of the task that may have increased as participants saw that their force level was not matching the instructions to remain at 50% MVC. The cerebellum is involved in predicting sensorimotor consequences of movements and in comparing the predictions to the actual sensory feedback (Popa & Ebner, 2018). Also, the cerebellum has little involvement with force production, but rather with kinematics of movements (Ebner et al., 2011) which is not a feature of our isometric task. Thus, the cerebellar BOLD increase could relate to the discrepancy between the amount of force participants were planning to generate and the actual output and this discrepancy increased as performance worsened. A complementary explanation is that the cerebellum activity was related to fatigue perception (Casamento-Moran et al., 2023).

The contralateral BOLD that remained high and stable throughout the blocks indicate that these areas were involved from the onset of the task most likely at peak capacity, at least within the confines of our methods. The ipsilateral BOLD increase has been shown before (Herath et al., 2010; Liu et al., 2003, 2007) and suggests that the brain was recruiting extra areas to match the task challenge and avoid fatigability. Liu et al. (2007) with an EEG study also proposed a shift of activity towards the ipsilateral hemisphere with fatigability development.

It might be surprising that we did not find fatigability-related BOLD changes in areas such as the contralateral sensorimotor areas, supplementary motor area, insula, or cingulate gyrus as prior work did (Benwell et al., 2007; Liu et al., 2002, 2003), especially considering that we did find fatigability-related EEG power increases in the C3 channel and others. First, we did show that BOLD in these areas was high and remained stable across blocks and we also found strong BOLD signal when the blocks were pooled which indicate that these areas were indeed involved during the task, but probably did not have fatigability-related influence as their activity remained constant across blocks. To explain this lack of change across blocks despite the change for EEG, one needs to consider that the origin of the EEG power differs from that of the BOLD signal. BOLD signal arises from enhanced

neuronal activity in a brain area (primarily the synaptic input and local processing rather than the output) which, in turn, increases the oxygen demand (Logothetis, 2008). EEG power is greatly influenced by the degree of synchronization of neuronal activity (Nunez & Srinivasan, 2006); for example, an increase in EEG power can be observed with an increase in synchrony even without an increase in neuronal activity (Cosandier-Rimele et al., 2008; Musall et al., 2014). Also, the metabolic demands are lower for a synchronized neuronal pool (Buzsaki & Draguhn, 2004). This could explain why we did not find BOLD changes while we did find EEG power increases. Also, intermittent tasks as we have here may lead to less BOLD changes than a sustained task (Liu et al., 2005). Finally, here we used a traditional fixed box car model of the HRF which is less complex than the EEG-informed fMRI analysis we implemented.

4.5. EEG-informed fMRI

To our knowledge, this is the first study to use EEG-informed fMRI to study fatigability. We used a richer HRF to estimate fatigability-related BOLD signal than the traditional fixed box car HRF (Fig. 1B), that is, we used the fluctuations of the EEG power, in different frequency bands, and for each participant separately. First, this showed that EEG predicted fMRI results in different frequency bands and with different polarity (Goldman et al., 2002; Kilner et al., 2005; Laufs et al., 2003; Scheeringa et al., 2016); that is, we found positive association for theta and negative association for the beta band.

Further, in the beta band this revealed areas that the traditional fMRI analysis with a fixed box car shape failed to reveal. In the beta band, this analysis revealed clusters in the left sensorimotor areas (straddling the primary motor cortex and somatosensory cortex) and anterior TPJ. In the right hemisphere, this analysis revealed a cluster straddling the supramarginal gyrus and anterior TPJ, and a cluster in the SMA/cingulate gyrus. These areas have been shown before to be involved with fatigability (Benwell et al., 2007; Post et al., 2009; van Duinen et al., 2007; Walitt et al., 2024). The EEG-fMRI negative relationship indicates that as EEG power increased (Fig. 4) BOLD decreased; we have shown that the BOLD signal in the three clusters decreased only slightly across all blocks (Supplementary Fig. S11B) which explains the negative association. Thus, it appears that with fatigability there was no significant increase of neuronal activity across blocks in these clusters, but rather an increase in neuronal activity synchronization as shown with EEG power. It might be that BOLD reached its maximum immediately at the 1st block and remained constant afterward, with a slight decrease. Of course, this is within the confines of our task and analysis as discussed in the *fMRI* section. For the theta band, this analysis revealed areas in the precuneus, lingual gyrus, and cerebellum. While these areas in the theta band only slightly overlapped with the cluster found in the first fMRI analysis (Fig. 5), they were contiguous with that cluster and probably should not be considered as new areas. We have discussed the role of these areas in the *fMRI* section.

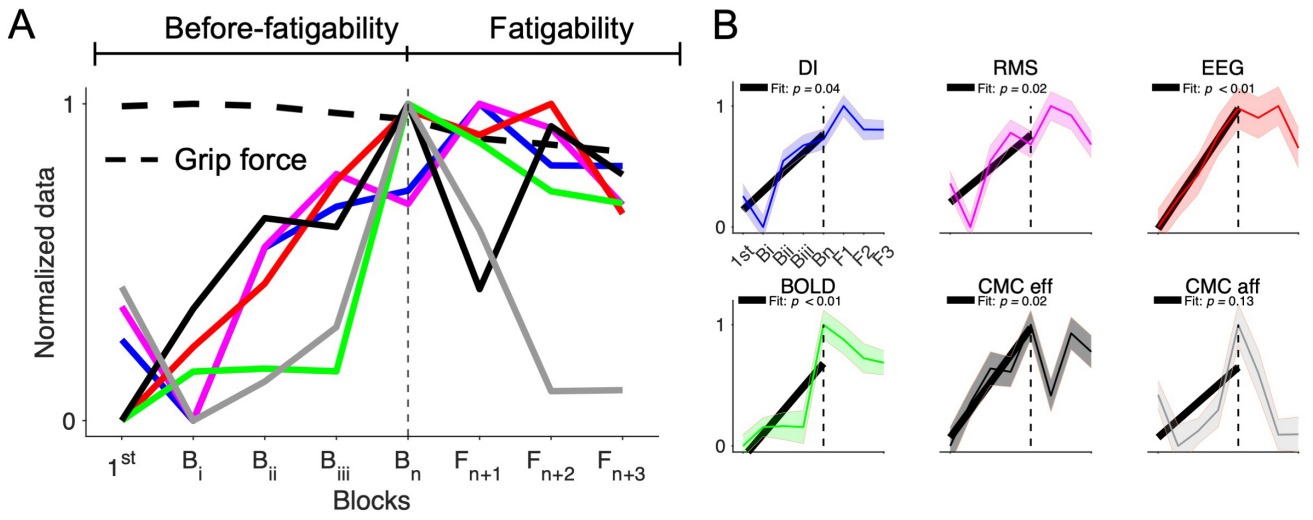

Fig. 9. Timeline of changes during fatigability development. (A) As grip force remained fairly constant up to the Bn block, changes in DI, RMS, EEG, and CMC efferent began much earlier and occurred together up to the Bn block. Changes in BOLD and CMC afferent occurred later. (B) Each metric (group mean ± s.e.m.) is fitted with linear regression for block 1st to Bn demonstrating that the increase was significant, but not for CMC aff. *DI:* Dimitrov Index*, RMS*: root mean square*, CMC*: corticomuscular coherence*, eff*: efferent, *aff*: afferent.

4.6. Neuromuscular changes precede fatigability

Before fatigability became manifest behaviorally at block B_n, we found that the neuromuscular system was already adapting to fatigability development. The muscles and the brain increased their output steadily from the 1st to the B_n block, most likely to try delaying fatigability. We found those effects in the muscles (EMG) and brain (EEG, fMRI), as well as the brain-muscles interaction (CMC). Those neuromuscular changes that preceded fatigability behavioral changes were also observed in fatigue while driving (Chuang et al., 2018).

To sum up the timeline of neuromuscular changes relative to fatigability development we plotted all metrics in Figure 9. We used the averages of each of the eight blocks as follows: DI: Figure 3C; RMS: Supplementary Fig. S1C; EEG in the mu band: Figure 4B; BOLD: average of the two cerebellar regions in Figure 5B; CMC efferent in the beta band: Figure 7C; CMC afferent in the beta band: Figure 7F. We first normalized each metric because they have different range of values. As can be seen in Figure 9A, before fatigability became manifest behaviorally as a decrease in grip force (blocks 1st to B_n), DI, RMS, EEG, and CMC efferent increased early during the task and in parallel. Changes in BOLD and CMC afferent occurred later. Once fatigability became manifest (blocks F_{n+1}, F_{n+2}, F_{n+3}), changes were less interconnected. In Figure 9B, we show each metric (mean ± s.e.m.) fitted with linear regression from the 1st to the B_n block to demonstrate the significant increase; the increase was not significant for CMC afferent.

5. CONCLUSION

Humans can generate enough forces to perform various tasks, but at some point, we reach a limit and the motor output decreases; this is when fatigability becomes behaviorally manifest. However, changes inside the neuromuscular system, that is, brain and muscles, have already taken place well before that limit. When fatigability became behaviorally manifest both the muscles and brain and their interaction have reached a peak of activity. A plethora of factors such as psychology (e.g., motivation, reward, personality), pain, and context (e.g., competition vs. recreational) will also influence fatigability development. Therefore, fatigability should be approached as a whole-body experience engaging muscles and brain simultaneously, rather than a binary problem of peripheral versus central. In all, fatigability helps to maintain homeostasis in the brain and muscles to prevent catastrophic depletion of resources and avoid brain and muscles damages due to exertion (Hureau et al., 2018; Mosso, 1915; Noakes, 2012). Our results in healthy volunteers will provide new insights into the typical neuromuscular process of fatigability and, in turn, better understand fatigability in diseases.

DATA AND CODE AVAILABILITY

Data and Code will be made available following appropriate request to the lead contact.

AUTHOR CONTRIBUTIONS

Conceptualization and Methodology: B.W., A.N., M.H., S.G.H., and T.P. Formal Analysis: P.B., K.M.K., P.M.M., S.G.H., and F.V. Investigation: P.B., K.M.K., P.M.M., S.G.H., F.V., and T.P. Data Curation: P.B., K.M.K., S.G.H., and P.M.M. Writing—Original Draft: P.B., K.M.K., S.G.H., T.P., M.H., and B.W. Writing—Review & Editing: P.B., K.M.K., S.G.H., T.P., M.H., and B.W. Visualization: P.B., S.G.H. Supervision: B.W., A.N., and M.H. Project Administration: B.W.

LEAD CONTACT

Requests for further information and resources should be directed to and will be fulfilled by the lead contact, Brian Walitt, brian.walitt@nih.gov.

FUNDING

This research was supported (in part) by the Intramural Research Program of the NIH, including National Institute of Neurological Diseases and Stroke (NINDS). Grant support for this project included: ZIA NS003157.

DECLARATION OF COMPETING INTEREST

The authors declare no competing interests.

SUPPLEMENTARY MATERIALS

Supplementary material for this article is available with the online version here: https://doi.org/10.1162/IMAG.a.132.

REFERENCES

Abreu, R., Leal, A., & Figueiredo, P. (2018). EEG-informed fMRI: A review of data analysis methods. *Front Hum Neurosci*, *12*, 29. https://doi.org/10.3389/fnhum.2018.00029

Allen, P. J., Josephs, O., & Turner, R. (2000). A method for removing imaging artifact from continuous EEG recorded during functional MRI. *Neuroimage*, *12*(2), 230–239. https://doi.org/10.1006/nimg.2000.0599

Amador-Tejada, A., McGillivray, J. E., Kumbhare, D. A., & Noseworthy, M. D. (2024). Denoising of the gradient

artifact present in simultaneous studies of muscle blood oxygen level dependent (BOLD) signal and electromyography (EMG). *Magn Reson Imaging*, *111*, 179–185. https://doi.org/10.1016/j.mri.2024.05.004

Amann, M., Blain, G. M., Proctor, L. T., Sebranek, J. J., Pegelow, D. F., & Dempsey, J. A. (2011). Implications of group III and IV muscle afferents for high-intensity endurance exercise performance in humans. *J Physiol*, *589*(Pt 21), 5299–5309. https://doi.org/10.1113/jphysiol.2011.213769

Amann, M., Venturelli, M., Ives, S. J., McDaniel, J., Layec, G., Rossman, M. J., & Richardson, R. S. (2013). Peripheral fatigue limits endurance exercise via a sensory feedback-mediated reduction in spinal motoneuronal output. *J Appl Physiol (1985)*, *115*(3), 355–364. https://doi.org/10.1152/japplphysiol.00049.2013

Amann, M., Wan, H. Y., Thurston, T. S., Georgescu, V. P., & Weavil, J. C. (2020). On the influence of Group III/IV muscle afferent feedback on endurance exercise performance. *Exerc Sport Sci Rev*, *48*(4), 209–216. https://doi.org/10.1249/JES.0000000000000233

Amjad, A. M., Halliday, D. M., Rosenberg, J. R., & Conway, B. A. (1997). An extended difference of coherence test for comparing and combining several independent coherence estimates: Theory and application to the study of motor units and physiological tremor. *J Neurosci Methods*, *73*(1), 69–79. https://doi.org/10.1016/S0165-0270(96)02214-5

Ataei, A., Amini, A., & Ghazizadeh, A. (2024). Robust memory of face moral values is encoded in the human caudate tail: A simultaneous EEG-fMRI study. *Sci Rep*, *14*(1), 12629. https://doi.org/10.1038/s41598-024-63085-w

Baker, S. N., Olivier, E., & Lemon, R. N. (1997). Coherent oscillations in monkey motor cortex and hand muscle EMG show task-dependent modulation. *J Physiol (Lond.)*, *501*(1), 225–241. https://doi.org/10.1111/j.1469-7793.1997.225bo.x

Beck, M. M., Spedden, M. E., & Lundbye-Jensen, J. (2021). Reorganization of functional and directed corticomuscular connectivity during precision grip from childhood to adulthood. *Sci Rep*, *11*(1), 22870. https://doi.org/10.1038/s41598-021-01903-1

Becker, R., Ritter, P., Moosmann, M., & Villringer, A. (2005). Visual evoked potentials recovered from fMRI scan periods. *Hum Brain Mapp*, *26*(3), 221–230. https://doi.org/10.1002/hbm.20152

Benjamini, Y., & Hochberg, Y. (1995). Controlling the false discovery rate: A practical and powerful approach to multiple testing. *J R Stat Soc Series B (Methodol)*, *57*(1), 289–300. https://doi.org/10.1111/j.2517-6161.1995.tb02031.x

Benwell, N. M., Mastaglia, F. L., & Thickbroom, G. W. (2007). Changes in the functional MR signal in motor and non-motor areas during intermittent fatiguing hand exercise. *Exp Brain Res*, *182*(1), 93–97. https://doi.org/10.1007/s00221-007-0973-5

Berchicci, M., Menotti, F., Macaluso, A., & Di Russo, F. (2013). The neurophysiology of central and peripheral fatigue during sub-maximal lower limb isometric contractions. *Front Hum Neurosci*, *7*, 135. https://doi.org/10.3389/fnhum.2013.00135

Bigland-Ritchie, B., Donovan, E. F., & Roussos, C. S. (1981). Conduction velocity and EMG power spectrum changes in fatigue of sustained maximal efforts. *J Appl Physiol Respir Environ Exerc Physiol*, *51*(5), 1300–1305. https://doi.org/10.1152/jappl.1981.51.5.1300

Buzsaki, G., & Draguhn, A. (2004). Neuronal oscillations in cortical networks. *Science*, *304*(5679), 1926–1929. https://doi.org/10.1126/science.1099745

Casamento-Moran, A., Mooney, R. A., Chib, V. S., & Celnik, P. A. (2023). Cerebellar excitability regulates physical fatigue perception. *J Neurosci*, *43*(17), 3094–3106. https://doi.org/10.1523/JNEUROSCI.1406-22.2023

Cavanna, A. E., & Trimble, M. R. (2006). The precuneus: A review of its functional anatomy and behavioural correlates. *Brain*, *129*, 564–583. https://doi.org/10.1093/brain/awl004

Chen, G., Saad, Z. S., Britton, J. C., Pine, D. S., & Cox, R. W. (2013). Linear mixed-effects modeling approach to FMRI group analysis. *Neuroimage*, *73*, 176–190. https://doi.org/10.1016/j.neuroimage.2013.01.047

Chuang, C. H., Cao, Z., King, J. T., Wu, B. S., Wang, Y. K., & Lin, C. T. (2018). Brain electrodynamic and hemodynamic signatures against fatigue during driving. *Front Neurosci*, *12*, 181. https://doi.org/10.3389/fnins.2018.00181

Conway, B. A., Halliday, D. M., Farmer, S. F., Shahani, U., Maas, P., Weir, A. I., & Rosenberg, J. R. (1995). Synchronization between motor cortex and spinal motoneuronal pool during the performance of a maintained motor task in man. *J Physiol (Lond.)*, *489*(3), 917–924. https://doi.org/10.1113/jphysiol.1995.sp021104

Cosandier-Rimele, D., Merlet, I., Badier, J. M., Chauvel, P., & Wendling, F. (2008). The neuronal sources of EEG: Modeling of simultaneous scalp and intracerebral recordings in epilepsy. *Neuroimage*, *42*(1), 135–146. https://doi.org/10.1016/j.neuroimage.2008.04.185

Delcamp, C., Gasq, D., Cormier, C., & Amarantini, D. (2023). Corticomuscular and intermuscular coherence are correlated after stroke: A simplified motor control? *Brain Commun*, *5*(3), fcad187. https://doi.org/10.1093/braincomms/fcad187

Delorme, A., & Makeig, S. (2004). EEGLAB: An open source toolbox for analysis of single-trial EEG dynamics including independent component analysis. *J Neurosci Methods*, *134*(1), 9–21. https://doi.org/10.1016/j.jneumeth.2003.10.009

Diedrichsen, J. (2006). A spatially unbiased atlas template of the human cerebellum. *Neuroimage*, *33*(1), 127–138. https://doi.org/10.1016/j.neuroimage.2006.05.056

Dimitrov, G. V., Arabadzhiev, T. I., Mileva, K. N., Bowtell, J. L., Crichton, N., & Dimitrova, N. A. (2006). Muscle fatigue during dynamic contractions assessed by new spectral indices. *Med Sci Sports Exerc*, *38*(11), 1971–1979. https://doi.org/10.1249/01.mss.0000233794.31659.6d

Dimitrova, N. A., Hogrel, J. Y., Arabadzhiev, T. I., & Dimitrov, G. V. (2005). Estimate of M-wave changes in human biceps brachii during continuous stimulation. *J Electromyogr Kinesiol*, *15*(4), 341–348. https://doi.org/10.1016/j.jelekin.2005.01.005

Dum, R. P., & Strick, P. L. (1996). Spinal cord terminations of the medial wall motor areas in macaque monkeys. *J Neurosci*, *16*(20), 6513–6525. https://doi.org/10.1523/JNEUROSCI.16-20-06513.1996

Ebner, T. J., Hewitt, A. L., & Popa, L. S. (2011). What features of limb movements are encoded in the discharge of cerebellar neurons? *Cerebellum*, *10*(4), 683–693. https://doi.org/10.1007/s12311-010-0243-0

Enders, H., Cortese, F., Maurer, C., Baltich, J., Protzner, A. B., & Nigg, B. M. (2016). Changes in cortical activity measured with EEG during a high-intensity cycling exercise. *J Neurophysiol*, *115*(1), 379–388. https://doi.org/10.1152/jn.00497.2015

Enoka, R. M., & Duchateau, J. (2016). Translating fatigue to human performance. *Med Sci Sports Exerc*, *48*(11), 2228–2238. https://doi.org/10.1249/Mss.0000000000000929

Gandevia, S. C. (2001). Spinal and supraspinal factors in human muscle fatigue. *Physiol Rev*, *81*(4), 1725–1789. https://doi.org/10.1152/physrev.2001.81.4.1725

Glories, D., Soulhol, M., Amarantini, D., & Duclay, J. (2021). Specific modulation of corticomuscular coherence during submaximal voluntary isometric, shortening and lengthening contractions. *Sci Rep*, *11*(1), 6322. https://doi.org/10.1038/s41598-021-85851-w

Goldman, R. I., Stern, J. M., Engel, J., Jr., & Cohen, M. S. (2002). Simultaneous EEG and fMRI of the alpha rhythm. *Neuroreport*, *13*(18), 2487–2492. https://doi.org/10.1097/01.wnr.0000047685.08940.d0

Guo, F., Wang, J. Y., Sun, Y. J., Yang, A. L., & Zhang, R. H. (2014). Movement-related cortical potentials during muscle fatigue induced by upper limb submaximal isometric contractions. *Neuroreport*, *25*(14), 1136–1143. https://doi.org/10.1097/WNR.0000000000000242

Gwin, J. T., & Ferris, D. P. (2012). Beta- and gamma-range human lower limb corticomuscular coherence. *Front Hum Neurosci*, *6*, 258. https://doi.org/10.3389/fnhum.2012.00258

Halliday, D. M. (2015). Nonparametric directionality measures for time series and point process data. *J Integr Neurosci*, *14*(2), 253–277. https://doi.org/10.1142/S0219635215300127

Halliday, D. M., Brittain, J. S., Stevenson, C. W., & Mason, R. (2018). Adaptive spectral tracking for coherence estimation: The z-tracker. *J Neural Eng*, *15*(2), 026004. https://doi.org/10.1088/1741-2552/aaa3b4

Halliday, D. M., Rosenberg, J. R., Amjad, A. M., Breeze, P., Conway, B. A., & Farmer, S. F. (1995). A framework for the analysis of mixed time series/point process data—Theory and application to the study of physiological tremor, single motor unit discharges and electromyograms. *Prog Biophys Mol Biol*, *64*(2–3), 237–278. https://doi.org/10.1016/s0079-6107(96)00009-0

Halliday, D. M., Senik, M. H., Stevenson, C. W., & Mason, R. (2016). Non-parametric directionality analysis—Extension for removal of a single common predictor and application to time series. *J Neurosci Methods*, *268*, 87–97. https://doi.org/10.1016/j.jneumeth.2016.05.008

Herath, P., Gallea, C., van der Veen, J. W., Horovitz, S. G., & Hallett, M. (2010). In vivo neurochemistry of primary focal hand dystonia: A magnetic resonance spectroscopic neurometabolite profiling study at 3T. *Mov Disord*, *25*(16), 2800–2808. https://doi.org/10.1002/mds.23306

Horovitz, S. G., Rossion, B., Skudlarski, P., & Gore, J. C. (2004). Parametric design and correlational analyses help integrating fMRI and electrophysiological data during face processing. *Neuroimage*, *22*(4), 1587–1595. https://doi.org/10.1016/j.neuroimage.2004.04.018

Hsu, L. I., Lim, K. W., Lai, Y. H., Chen, C. S., & Chou, L. W. (2023). Effects of muscle fatigue and recovery on the neuromuscular network after an intermittent handgrip fatigue task: Spectral analysis of electroencephalography and electromyography signals. *Sensors (Basel)*, *23*(5), 2440. https://doi.org/10.3390/s23052440

Hureau, T. J., Romer, L. M., & Amann, M. (2018). The 'sensory tolerance limit': A hypothetical construct determining exercise performance? *Eur J Sport Sci*, *18*(1), 13–24. https://doi.org/10.1080/17461391.2016.1252428

Igelström, K. M., & Graziano, M. S. A. (2017). The inferior parietal lobule and temporoparietal junction: A network perspective. *Neuropsychologia*, *105*, 70–83. https://doi.org/10.1016/j.neuropsychologia.2017.01.001

Jiang, Z., Wang, X. F., & Yue, G. H. (2016). Strengthened corticosubcortical functional connectivity during muscle fatigue. *Neural Plast*, *2016*, 1726848. https://doi.org/10.1155/2016/1726848

Jo, H. J., Saad, Z. S., Simmons, W. K., Milbury, L. A., & Cox, R. W. (2010). Mapping sources of correlation in resting state FMRI, with artifact detection and removal. *Neuroimage*, *52*(2), 571–582. https://doi.org/10.1016/j.neuroimage.2010.04.246

Johnston, J., Rearick, M., & Slobounov, S. (2001). Movement-related cortical potentials associated with progressive muscle fatigue in a grasping task. *Clin Neurophysiol*, *112*(1), 68–77. https://doi.org/10.1016/s1388-2457(00)00452-1

Kilner, J. M., Mattout, J., Henson, R., & Friston, K. J. (2005). Hemodynamic correlates of EEG: A heuristic. *Neuroimage*, *28*(1), 280–286. https://doi.org/10.1016/j.neuroimage.2005.06.008

Kluger, B. M., Krupp, L. B., & Enoka, R. M. (2013). Fatigue and fatigability in neurologic illnesses: Proposal for a unified taxonomy. *Neurology*, *80*(4), 409–416. https://doi.org/10.1212/WNL.0b013e31827f07be

Kristeva, R., Patino, L., & Omlor, W. (2007). Beta-range cortical motor spectral power and corticomuscular coherence as a mechanism for effective corticospinal interaction during steady-state motor output. *Neuroimage*, *36*(3), 785–792. https://doi.org/10.1016/j.neuroimage.2007.03.025

Laufs, H., Kleinschmidt, A., Beyerle, A., Eger, E., Salek-Haddadi, A., Preibisch, C., & Krakow, K. (2003). EEG-correlated fMRI of human alpha activity. *Neuroimage*, *19*(4), 1463–1476. https://doi.org/10.1016/s1053-8119(03)00286-6

Laurin, J., Pertici, V., Dousset, E., Marqueste, T., & Decherchi, P. (2015). Group III and IV muscle afferents: Role on central motor drive and clinical implications. *Neuroscience*, *290*, 543–551. https://doi.org/10.1016/j.neuroscience.2015.01.065

Liang, T., Zhang, Q., Hong, L., Liu, X., Dong, B., Wang, H., & Liu, X. (2021). Directed information flow analysis reveals muscle fatigue-related changes in muscle networks and corticomuscular coupling. *Front Neurosci*, *15*, 750936. https://doi.org/10.3389/fnins.2021.750936

Liu, J., Sheng, Y., & Liu, H. (2019). Corticomuscular coherence and its applications: A review. *Front Hum Neurosci*, *13*, 100. https://doi.org/10.3389/fnhum.2019.00100

Liu, J. Z., Dai, T. H., Sahgal, V., Brown, R. W., & Yue, G. H. (2002). Nonlinear cortical modulation of muscle fatigue: A functional MRI study. *Brain Res*, *957*(2), 320–329. https://doi.org/10.1016/s0006-8993(02)03665-x

Liu, J. Z., Lewandowski, B., Karakasis, C., Yao, B., Siemionow, V., Sahgal, V., & Yue, G. H. (2007). Shifting of activation center in the brain during muscle fatigue: An explanation of minimal central fatigue? *Neuroimage*, *35*(1), 299–307. https://doi.org/10.1016/j.neuroimage.2006.09.050

Liu, J. Z., Shan, Z. Y., Zhang, L. D., Sahgal, V., Brown, R. W., & Yue, G. H. (2003). Human brain activation during sustained and intermittent submaximal fatigue muscle contractions: An FMRI study. *J Neurophysiol*, *90*(1), 300–312. https://doi.org/10.1152/jn.00821.2002

Liu, J. Z., Zhang, L. D., Yao, B., Sahgal, V., & Yue, G. H. (2005). Fatigue induced by intermittent maximal voluntary contractions is associated with significant losses in muscle output but limited reductions in functional MRI-measured brain activation level. *Brain Res*, *1040*(1–2), 44–54. https://doi.org/10.1016/j.brainres.2005.01.059

Logothetis, N. (2008). What we can do and what we cannot do with fMRI. *Nature*, *453*, 869–878. https://doi.org/10.1038/nature06976

McClelland, V. M., Cvetkovic, Z., & Mills, K. R. (2012). Modulation of corticomuscular coherence by peripheral stimuli. *Exp Brain Res*, *219*(2), 275–292. https://doi.org/10.1007/s00221-012-3087-7

Mehrkanoon, S., Breakspear, M., & Boonstra, T. W. (2014). The reorganization of corticomuscular coherence during a transition between sensorimotor states. *Neuroimage*, *100*, 692–702. https://doi.org/10.1016/j.neuroimage.2014.06.050

Mendez-Balbuena, I., Naranjo, J. R., Wang, X., Andrykiewicz, A., Huethe, F., Schulte-Monting, J., Hepp-Reymond, M. C., & Kristeva, R. (2013). The strength of the corticospinal coherence depends on the predictability of modulated isometric forces. *J Neurophysiol*, *109*(6), 1579–1588. https://doi.org/10.1152/jn.00187.2012

Merletti, R., Aventaggiato, M., Botter, A., Holobar, A., Marateb, H., & Vieira, T. M. (2010). Advances in surface EMG: Recent progress in detection and processing techniques. *Crit Rev Biomed Eng*, *38*(4), 305–345. https://doi.org/10.1615/critrevbiomedeng.v38.i4.10

Millet, G. Y., Bertrand, M. F., Lapole, T., Feasson, L., Rozand, V., & Hupin, D. (2023). Measuring objective fatigability and autonomic dysfunction in clinical populations: How and why? *Front Sports Act Living*, *5*, 1140833. https://doi.org/10.3389/fspor.2023.1140833

Mima, T., & Hallett, M. (1999). Corticomuscular coherence: A review. *J Clin Neurophysiol*, *16*(6), 501–511. https://doi.org/10.1097/00004691-199911000-00002

Mosso, A. (1915). *Fatigue*. Allen and Unwin. https://www.google.co.in/books/edition/Fatigue/WzEIHQAACAAJ?hl=en

Musall, S., von Pfostl, V., Rauch, A., Logothetis, N. K., & Whittingstall, K. (2014). Effects of neural synchrony on surface EEG. *Cereb Cortex*, *24*(4), 1045–1053. https://doi.org/10.1093/cercor/bhs389

Neto, O. P., & Christou, E. A. (2010). Rectification of the EMG signal impairs the identification of oscillatory input to the muscle. *J Neurophysiol*, *103*(2), 1093–1103. https://doi.org/10.1152/jn.00792.2009

Noakes, T. D. (2012). Fatigue is a brain-derived emotion that regulates the exercise behavior to ensure the protection of whole body homeostasis. *Front Physiol*, *3*, 82. https://doi.org/10.3389/fphys.2012.00082

Nunez, P. L., & Srinivasan, R. (2006). *Electric fields of the brain: The neurophysics of EEG*. Oxford University Press. https://doi.org/10.1093/acprof:oso/9780195050387.001.0001

Omlor, W., Patino, L., Mendez-Balbuena, I., Schulte-Mönting, J., & Kristeva, R. (2011). Corticospinal beta-range coherence is highly dependent on the pre-stationary motor state. *J Neurosci*, *31*(22), 8037–8045. https://doi.org/10.1523/Jneurosci.4153-10.2011

Patino, L., Omlor, W., Chakarov, V., Hepp-Reymond, M. C., & Kristeva, R. (2008). Absence of gamma-range corticomuscular coherence during dynamic force in a deafferented patient. *J Neurophysiol*, *99*(4), 1906–1916. https://doi.org/10.1152/jn.00390.2007

Piper, H. (1912). *Elektrophysiologie menschlicher muskeln*. Springer. https://doi.org/10.1007/978-3-642-50944-5

Popa, L. S., & Ebner, T. J. (2018). Cerebellum, predictions and errors. *Front Cell Neurosci*, *12*, 524. https://doi.org/10.3389/fncel.2018.00524

Post, M., Steens, A., Renken, R., Maurits, N. M., & Zijdewind, I. (2009). Voluntary activation and cortical activity during a sustained maximal contraction: An fMRI study. *Hum Brain Mapp*, *30*(3), 1014–1027. https://doi.org/10.1002/hbm.20562

Puce, L., Pallecchi, I., Marinelli, L., Mori, L., Bove, M., Diotti, D., Ruggeri, P., Faelli, E., Cotellessa, F., & Trompetto, C. (2021). Surface electromyography spectral parameters for the study of muscle fatigue in swimming. *Front Sports Act Living*, *3*, 644765. https://doi.org/10.3389/fspor.2021.644765

Ritter, P., Becker, R., Graefe, C., & Villringer, A. (2007). Evaluating gradient artifact correction of EEG data acquired simultaneously with fMRI. *Magn Reson Imaging*, *25*(6), 923–932. https://doi.org/10.1016/j.mri.2007.03.005

Scheeringa, R., Koopmans, P. J., van Mourik, T., Jensen, O., & Norris, D. G. (2016). The relationship between oscillatory EEG activity and the laminar-specific BOLD signal. *Proc Natl Acad Sci U S A*, *113*(24), 6761–6766. https://doi.org/10.1073/pnas.1522577113

Schillings, M. L., Kalkman, J. S., van der Werf, S. P., Bleijenberg, G., van Engelen, B. G., & Zwarts, M. J. (2006). Central adaptations during repetitive contractions assessed by the readiness potential. *Eur J Appl Physiol*, *97*(5), 521–526. https://doi.org/10.1007/s00421-006-0211-z

Sidhu, S. K., Weavil, J. C., Mangum, T. S., Jessop, J. E., Richardson, R. S., Morgan, D. E., & Amann, M. (2017). Group III/IV locomotor muscle afferents alter motor cortical and corticospinal excitability and promote central fatigue during cycling exercise. *Clin Neurophysiol*, *128*(1), 44–55. https://doi.org/10.1016/j.clinph.2016.10.008

Sidhu, S. K., Weavil, J. C., Thurston, T. S., Rosenberger, D., Jessop, J. E., Wang, E., Richardson, R. S., McNeil, C. J., & Amann, M. (2018). Fatigue-related group III/IV muscle afferent feedback facilitates intracortical inhibition during locomotor exercise. *J Physiol*, *596*(19), 4789–4801. https://doi.org/10.1113/JP276460

Siemionow, V., Sahgal, V., & Yue, G. H. (2010). Single-Trial EEG-EMG coherence analysis reveals muscle fatigue-related progressive alterations in corticomuscular coupling. *IEEE Trans Neural Syst Rehabil Eng*, *18*(2), 97–106. https://doi.org/10.1109/TNSRE.2010.2047173

Spedden, M. E., Jensen, P., Terkildsen, C. U., Jensen, N. J., Halliday, D. M., Lundbye-Jensen, J., Nielsen, J. B., & Geertsen, S. S. (2019). The development of functional and directed corticomuscular connectivity during tonic ankle muscle contraction across childhood and adolescence. *Neuroimage*, *191*, 350–360. https://doi.org/10.1016/j.neuroimage.2019.02.054

Sun, J., Liu, G., Sun, Y., Lin, K., Zhou, Z., & Cai, J. (2022). Application of surface electromyography in exercise fatigue: A review. *Front Syst Neurosci*, *16*, 893275. https://doi.org/10.3389/fnsys.2022.893275

Suviseshamuthu, E. S., Shenoy Handiru, V., Allexandre, D., Hoxha, A., Saleh, S., & Yue, G. H. (2022). EEG-based spectral analysis showing brainwave changes related to modulating progressive fatigue during a prolonged intermittent motor task. *Front Hum Neurosci*, *16*, 770053. https://doi.org/10.3389/fnhum.2022.770053

Taylor, J. L., Amann, M., Duchateau, J., Meeusen, R., & Rice, C. L. (2016). Neural contributions to muscle fatigue: From the brain to the muscle and back again. *Med Sci Sports Exerc*, *48*(11), 2294–2306. https://doi.org/10.1249/Mss.0000000000000923

Tecchio, F., Porcaro, C., Zappasodi, F., Pesenti, A., Ercolani, M., & Rossini, P. M. (2006). Cortical short-term fatigue effects assessed via rhythmic brain-muscle coherence. *Exp Brain Res*, *174*(1), 144–151. https://doi.org/10.1007/s00221-006-0432-8

Tuncel, D., Dizibuyuk, A., & Kiymik, M. K. (2010). Time frequency based coherence analysis between EEG and EMG activities in fatigue duration. *J Med Syst*, *34*(2), 131–138. https://doi.org/10.1007/s10916-008-9224-y

Ushiyama, J., Katsu, M., Masakado, Y., Kimura, A., Liu, M., & Ushiba, J. (2011). Muscle fatigue-induced enhancement of corticomuscular coherence following sustained submaximal isometric contraction of the tibialis anterior muscle. *J Appl Physiol (1985)*, *110*(5), 1233–1240. https://doi.org/10.1152/japplphysiol.01194.2010

Ushiyama, J., Yamada, J., Liu, M., & Ushiba, J. (2017). Individual difference in beta-band corticomuscular coherence and its relation to force steadiness during isometric voluntary ankle dorsiflexion in healthy humans. *Clin Neurophysiol*, *128*(2), 303–311. https://doi.org/10.1016/j.clinph.2016.11.025

van Duinen, H., Renken, R., Maurits, N., & Zijdewind, I. (2007). Effects of motor fatigue on human brain activity, an fMRI study. *Neuroimage*, *35*(4), 1438–1449. https://doi.org/10.1016/j.neuroimage.2007.02.008

Walitt, B., Singh, K., LaMunion, S. R., Hallett, M., Jacobson, S., Chen, K., Enose-Akahata, Y., Apps, R., Barb, J. J., Bedard, P., Brychta, R. J., Buckley, A. W., Burbelo, P. D., Calco, B., Cathay, B., Chen, L., Chigurupati, S., Chen, J., Cheung, F., … Nath, A. (2024). Deep phenotyping of post-infectious myalgic encephalomyelitis/chronic fatigue syndrome. *Nat Commun*, *15*(1), 907. https://doi.org/10.1038/s41467-024-45107-3

Wan, J. J., Qin, Z., Wang, P. Y., Sun, Y., & Liu, X. (2017). Muscle fatigue: General understanding and treatment. *Exp Mol Med*, *49*(10), e384. https://doi.org/10.1038/emm.2017.194

Wang, Y., Cao, L., Hao, D., Rong, Y., Yang, L., Zhang, S., Chen, F., & Zheng, D. (2017). Effects of force load, muscle fatigue and extremely low frequency magnetic stimulation on EEG signals during side arm lateral raise task. *Physiol Meas*, *38*(5), 745–758. https://doi.org/10.1088/1361-6579/aa6b4b

Warbrick, T. (2022). Simultaneous EEG-fMRI: What have we learned and what does the future hold? *Sensors*, *22*(6), 2262. https://doi.org/10.3390/s22062262

Witham, C. L., Riddle, C. N., Baker, M. R., & Baker, S. N. (2011). Contributions of descending and ascending pathways to corticomuscular coherence in humans. *J Physiol*, *589*(Pt 15), 3789–3800. https://doi.org/10.1113/jphysiol.2011.211045

Yang, Q., Fang, Y., Sun, C. K., Siemionow, V., Ranganathan, V. K., Khoshknabi, D., Davis, M. P., Walsh, D., Sahgal, V., & Yue, G. H. (2009). Weakening of functional corticomuscular coupling during muscle fatigue. *Brain Res*, *1250*, 101–112. https://doi.org/10.1016/j.brainres.2008.10.074

Zhao, H., Nishioka, T., & Okada, J. (2022). Validity of using perceived exertion to assess muscle fatigue during resistance exercises. *Peerj*, *10*, e13019. https://doi.org/10.7717/peerj.13019